Multifractal Cascade Dynamics and Turbulent Intermittency

D. Schertzer
Laboratoire de Modélisation en Mécanique[a]*, Université Pierre et Marie Curie, Paris, France.*

S. Lovejoy
Physics Department, McGill University, Montreal, Canada

F. Schmitt
Institut Royal Météorologique, Brussels, Belgium

Y. Chigirinskaya, D. Marsan
Laboratoire de Modélisation en Mécanique, Université Pierre et Marie Curie[a]*, Paris, France*

Turbulent intermittency plays a fundamental role in fields ranging from combustion physics, chemical engineering to meteorology. There is a rather general agreement that multifractals are being very successful at quantifying this intermittency. However, we argue that cascade processes are the appropriate and necessary physical models to achieve dynamical modeling of turbulent intermittency. We first review some recent developments and point out new directions which overcome either completely or partially the limitations of current cascade models which are static, discrete in scale, acausal, purely phenomenological and lacking in universal features. We review the debate about universality classes for multifractal processes. Using both turbulent velocity and temperature data, we show that the latter are very well fitted by the (strong) universality, and that the recent (weak, log-Poisson) alternative is untenable for both strong and weak events. Using a continuous, space-time anisotropic framework, we then show how to produce a causal stochastic model of intermittent fields and use it to study the predictability of these fields. Finally, by returning to the origins of the turbulent "shell models" and restoring a large number of degrees of freedom (the Scaling Gyroscope Cascade, SGC models) we partially close the gap between the cascades and the dynamical Navier-Stokes equations. Furthermore, we point out that beyond a close agreement between universal parameters of the different modeling approaches and the empirical estimates in turbulence, there is a rather common structure involving both a "renormalized viscosity" and a "renormalized forcing". We conclude that this gives credence to the possibility of deriving analytical/renormalized models of intermittency built on this structure.

[a] On leave from Laboratoire de Météorologie Dynamique, Université Pierre et Marie Curie, Paris, France

1 Introduction

1.1 Why we need cascades

Turbulence is without any doubt one of the most challenging and presumably also one of the most frustrating problems for chemical engineering. It seems rather peculiar that so many practical issues still depend on a paradigm going back at least since Richardson's famous poem [1]: the paradigm of of turbulent cascades. It is already remarkable that a rather immediate developments of this paradigm lead to the first quantitative law of turbulence: the Richardson law of turbulent diffusion [2].

It took nearly 20 years before Kolmogorov exploited cascades to derive [3] the scaling law for the velocity field itself. Basing himself on three statistical hypotheses, Kolmogorov postulated a "quasi-equilibrium" for turbulence. The rate of large scale forcing energy (at outer scale L) leads to a flux of energy flowing through the "inertial range" of intermediate scales ℓ ($L >> \ell >> \eta$) towards small scales, where (at a small "Kolmogorov scale" η) it is dissipated. In the quasi-equilibrium regime the three quantities should be equal, at least for an appropriate average. The dynamics of this inertial range are therefore explicitly dominated by an invariant which was only casually included in Richardson's law: the flux of energy ε. More precisely, its average $\overline{\varepsilon}$ was considered. This yields the famous $\frac{2}{3}$ Kolmogorov law which states that shears across eddies/structures (ℓ being the scale, the angle brackets indicate ensemble averages) scale with this $\frac{2}{3}$ exponent:

$$< (\Delta u_\ell)^2 > \propto \overline{\varepsilon}^{\frac{2}{3}} \ell^{\frac{2}{3}} \tag{1}$$

This corresponds to the even more famous scaling law, derived by Obukhov [4] for the energy spectrum ($E(k)$, k being the wave-number)

$$E(k) \propto \overline{\varepsilon}^{\frac{2}{3}} k^{-\frac{5}{3}} \tag{2}$$

1.2 Analytic approaches to turbulence: closures and renormalization

It is remarkable that for over fifty years very little progress has been made in improving the (nearly hand-waving) original Richardson and Kolmogorov arguments. This is true in spite of the development of powerful analytical tools, including the Quasi Normal Approximation [5], the Direct Interaction Approximation [6,7] and numerous related analytical "closure" techniques (for this and related methods, see [8,9] for reviews). This also includes various applications of the Renormalization Group [10]. These techniques share a similar structure which could be called "renormalized viscosity/renormalized forcing"

since, in their framework, both terms correspond [59] to the leading contributions from other scales to the evolution of a given scale. Whereas the notion of eddy/renormalized viscosity could be traced back to the notion of mixing length [11], the notion of renormalized forcing seems rather recent and due to the development of these techniques. The equation of evolution of a Fourier component of the velocity ($\underline{\hat{u}}(\underline{k},t)$, $\underline{k}$ being its wave-vector) follows an equation of evolution of the type:

$$[\frac{\partial}{\partial t} + \nu_R(\underline{k},t)k^2]\underline{\hat{u}}(\underline{k},t) = \underline{\hat{f}}_R(\underline{k},t) \tag{3}$$

where ν_R is the renormalized viscosity and $\underline{\hat{f}}_R$ is the renormalized forcing ($\hat{\cdot}$ denotes the Fourier Transform) which is usually assumed to be quasi-Gaussian. However, without appeal to artificial ad hoc hypotheses, these attempts have led neither to satisfactory derivations of the Richardson nor Kolmogorov laws. The failure of these analytic approaches is even more striking since it was soon realized that both are at best "mean field" laws. In other words even these lowest order laws are still beyond the reach of present analytical developments! Indeed, these problems can be traced to the presence of a very strong type of inhomogeneity called "intermittency" (as first pointed out by Landau [12] and Batchelor and Townsend [13]). Not only does the "activity" of turbulence induce inhomogeneity, but the activity itself is inhomogeneously distributed. There are "puffs" of (active) turbulence inside "puffs" of (active) turbulence.

While these analytic attempts have yielded some insight into the structure of the Navier-Stokes equations and the first basic feature of turbulence - its scaling [b] - they have been totally unable to handle its intermittency (e.g. [14]). It is becoming increasingly clear that this second feature is neither secondary nor - as is too often suggested (e.g. the expression "intermittency corrections") - second order. Indeed, although it was less and less explicitly stated, analytical theories have remained more or less quasi-normal and have therefore been unable to deal with probability distributions as wild as those of a log-normal or algebraic type (not to mention the simple idea of puffs of activity inside of puffs of activity).

It should now be no surprise that the cascade paradigm not only provides a convenient framework to study this phenomenology, but furthermore yields very concrete models and interesting conjectures. In particular, it is now increasingly clear that a very general outcome of stochastic cascades is multifractal measures. While the discussion of various precise features of stochastic multifractals are the main subject of this paper (Secs. 2-4), Sec. 5 shows that

[b] Notwithstanding they fail, as mentioned above, to overcome fundamental difficulties in deriving the correct scaling law.

even deterministic cascades (restrictions of which form the popular "shell models") also yield multifractals.

In spite of their rather distinct origins, we will see (Secs. 4-5) that these techniques are all rather closely related to the renormalized viscosity/renormalized forcing structure of the analytical/renormalization techniques that we mentioned above (Eq. 3). We will therefore point out that contrary to certain claims (e.g. [60]) there is the possibility of deriving an analytical/renormalized model of intermittency. In order to emphasize the crucial importance of explicit models, let us briefly recall a further historical point. The first concrete conjecture on intermittency -the so-called log-normal probability distribution [15,16] for the rate of energy dissipation ε was formulated with reference to the notion of cascades, but without any concrete model. It was only after the development of an early explicit model [17] that the relevance of log-normality became contested (Sec. 2.2).

1.3 Low dimensional/deterministic chaos and universality

Another approach to turbulence which has received great attention (especially) in the last twenty years, is deterministic chaos. Although the word "chaos" goes back to the Greeks, it has only been in this recent period that it has taken on a highly restrictive meaning involving deterministic systems with small numbers of degrees of freedom. Initially Lorenz [18], proposed chaos as an interesting mathematical caricature of convection. The discovery first of "structural" and then of "metric" universality [19] led to an explosion of interest in chaotic dynamics: the caricatures could yield some fundamental features of wide classes of physical systems.

Applications of chaos theory were subsequently given a big impetus with the discovery of practical methods for "reconstructing" the strange attractor from time series data (e.g. the Grassberger-Proccaccia algorithm [20]). However, it became clear that such techniques are inherently incapable of distinguishing between low dimensional deterministic systems and high dimensional stochastic systems ("stochastic chaos", see below), whereas the former case is a condition of applicability of the corresponding methods, if not of the theory. It has become widely recognized that a small number of degrees of freedom model is inadequate for turbulence (Fig.1a-b), except perhaps in the low Reynolds number regime near (but below) the transition to turbulence.

However, for essentially the same reasons as for chaotic systems, cascades and their resulting multifractal fields (summarized in Sec. 2) would be physically unmanageable if not for the existence of universality classes [21–23]. In their absence, multifractal models would involve an infinite number of parameters

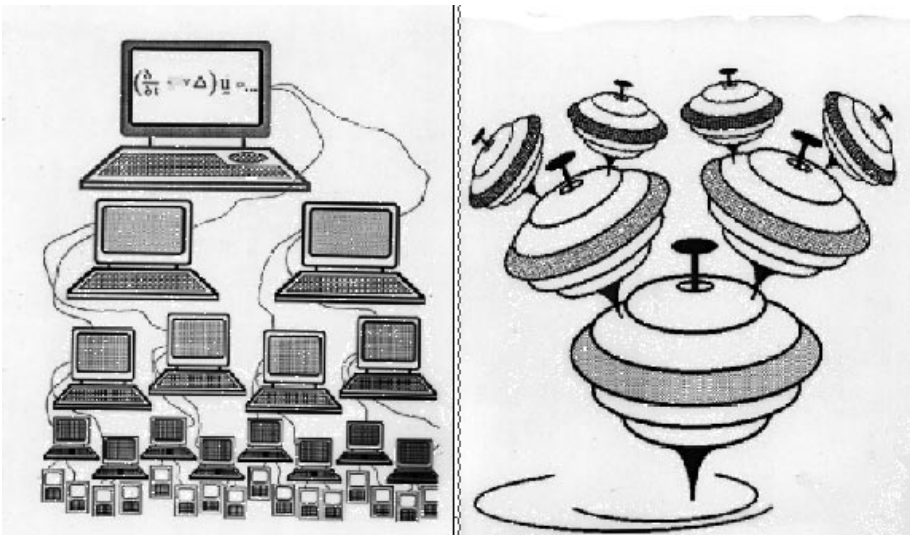

Figure 1: a) A fundamental problem in turbulence is that the number of degrees of freedom increases algebraically as we go to smaller and smaller scales. Direct numerical simulations of fully developed turbulence would therefore require a cascade of computers as illustrated above, i.e. a scale by scale iteration (and radical extension) of the meteorologists' idea of "nested" models. b) While for direct simulations, this may be out of reach for the next few decades, this is easily accessible for cascades models in particular for "the Scaling Gyroscopes Cascade" (illustrated above) which is rather illustrative of Richardson's poem, since it corresponds[52] to big tops have little tops which feed on their momentum and little top have smaller tops...

(e.g. the fractal codimensions). On the one hand, all the details of the model would be important, while on the other hand it would be impossible to empirically determine an infinite number of parameters. The existence of stable, attractive universality classes ("strong universality") has - starting with [24,25] - now been empirically confirmed in over twenty turbulent fields (for a review [26]). Recently, a weaker type of universality has been proposed [27–30]. Sec. 3 provides a detailed empirical intercomparison of the (somewhat classical) strong (Lévy generator) universality [31–33] with the weak (Poisson generator) universality using both turbulent velocity and temperature data. We find - although both agree well with the data for the medium intensity fluctuations - that for both the weak and strong fluctuations the classical strong universality is much closer to the data than the weak alternative. We further add new theoretical arguments why strong universality is relevant for passive scalar advection.

1.4 Stochastic chaos and temporal multifractal modelling

While cascades are indeed the generic multifractal process, due to the existence of thermodynamic analogues [34–36], multifractals can also be formulated as an abstract (model independent) "flux dynamics" [37,38]. However for many applications, it is important to have explicit (constructive) multifractal models. These are stochastic and therefore can provide phenomenological models for many large number of degrees of freedom systems including turbulence; calling them "stochastic chaos" might be more appropriate than the term "edge of chaos" (referring to the Lyapunov exponents equal to zero in scaling systems).

The first generation of cascade models was static (purely in the spatial domain) and involved discrete, integer scale ratios. These include "the pulse in pulse model" [39], the "log-normal model" [17], the "weighted curdling model" [40], the "β-model" [41], the "α-model" [42], the "random β-model" [43], the "p-model" [44], "Synthetic turbulence" [45], etc. Second generation, more realistic cascades, are on the contrary continuous in scale [21] (see [46] for numerical implementation). However since most turbulent systems are scaling but anisotropic, full realism requires at least spatial anisotropy. Furthermore, since the temporal and spatial scaling exponents are different, space-time anisotropy is required to model temporal evolution. The basic framework necessary to handle such scaling anisotropy - Generalized Scale Invariance [47,37] (see [48,49] for numerical implementation) - is straightforward, and space-time multifractals have already been explored in the film "Multifractal dynamics" [50].

These second generation space-time models still have a significant weakness. While they do have the correct space-time stratification, they do not respect causality: the future remains statistically symmetric with the past.

This artificial time mirror-symmetry is broken [51] as soon as one considers a (generalized) diffusion equation (of fractional spatial and temporal order) for the singularities (i.e. for the cascade generator). In Sec. 4, we review this and show how these continuous, causal, space-time multifractal models can be used to study the limits to predictability of multifractal processes. These results are important for developing multifractal forecasting procedures which promise applications in weather forecasting (especially nowcasting), and elsewhere.

1.5 Deterministic high dimensional models

Although stochastic multifractal cascade models of turbulence respect various symmetries of the dynamical equations - notably the scaling and the energy flux conservation, there is nonetheless a large gap between the deterministic Navier-Stokes equations for the (vector) velocity field and these phenomenological cascades for the (scalar) energy flux.

An extension to vector cascades [109], called "Lie cascades", has been considered in order to bridge the gap. However, in this framework, the extra symmetries which must be respected are not yet known. As discussed in Sec. 5, a deterministic cascade called the Scaling Gyroscopes Cascade (SGC) model [52] is likely to be be indispensable in overcoming this difficulty. This approach is inspired by similarities between the Navier-Stokes equations of hydrodynamic turbulence and the Euler equations of a gyroscope which have been noted since at least Lamb [53], and were given new impetus by Arnold [54] and Obukhov [55]. We discuss a precise series of approximations to the Navier-Stokes equations which yield SGC for respectively 3-D and 2-D turbulence. The resulting SGC model is a "model of hydrodynamic type" [55] having the same scaling symmetries and quadratic invariants as Navier-Stokes and the same Lie structure for a sub-set of interactions. Furthermore, we find that it has nearly exactly the same universal multifractal behaviour as the empirical energy flux. On the contrary, a rather different multifractality is obtained for the shell-model which is derived by over-simplifying the SGC, as done [56] on a similar model yielding the ancestor [57,58] of shell-models. The quantitative difference between the high dimensional SGC and the derived low dimensional shell-model brings into question the relevance of the (popular) shell-models for investigating intermittency.

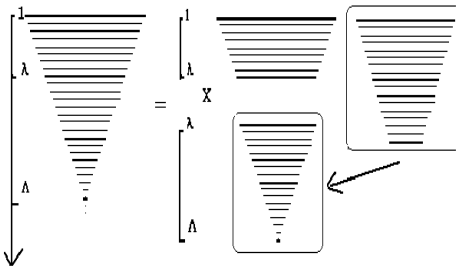

Figure 2: Scheme of a multiplicative (discrete) cascade, the horizontal lines symbolize the scales involved. The process from the outer scale L to $\frac{L}{\Lambda}$, with the scale ratio $\Lambda = \lambda\lambda'$, is the product of two sub-cascades, the first one occurs from the outer scale L to $\frac{L}{\lambda}$, whereas the second is a rescaled version (by scale ratio λ) of a cascade developed from L to $\frac{L}{\lambda'}$.

2 Fundamental properties of multifractal processes

2.1 Multiscaling of moments and probabilities

Dimension and codimension formalisms

Multifractal processes originated from the phenomenological assumption (Fig. 2 for illustration) that in turbulence the successive cascade steps define the fraction of the flux transmitted to smaller scales and that a cascade from scale ratio λ to scale ratio $\Lambda = \lambda\lambda'$ is a rescaled version (by scale ratio λ) of a cascade from ratio 1 to λ'. To fix the ideas, consider a square domain of size $L \times L$, characterized by an intensity ε_0, and at any given step n one divides the existing structures at scale $l_{n-1} = \frac{L}{\lambda_1^{n-1}}$ with intensities ε_{n-1} into λ_1^2 new structures at scale $l_n = \frac{l_{n-1}}{\lambda_1} = \frac{L}{\lambda_1^n}$ with intensities $\varepsilon_n = \varepsilon_{n-1} \times \mu\varepsilon$ where λ_1 is an integer and the multiplicative increment $\mu\varepsilon$ is a positive random variable with a second Laplace characteristic function $K(q)$ such that $\langle \mu\varepsilon^q \rangle = \lambda_1^{K(q)}$. The iteration of this generator leads, after N steps ($\Lambda = \lambda_1^N$), to an intermittent field with $\langle \varepsilon_\Lambda^q \rangle = \Lambda^{K(q)}$. Fig. 3 shows such a procedure (with the changes of notation: $L \rightarrow l_0$ and $\lambda_1 \rightarrow \lambda$).

A continuous version of this model (i.e. in the limit $\lambda_1 \rightarrow 1$ keeping Λ constant) would be characterized by its statistical invariance properties for

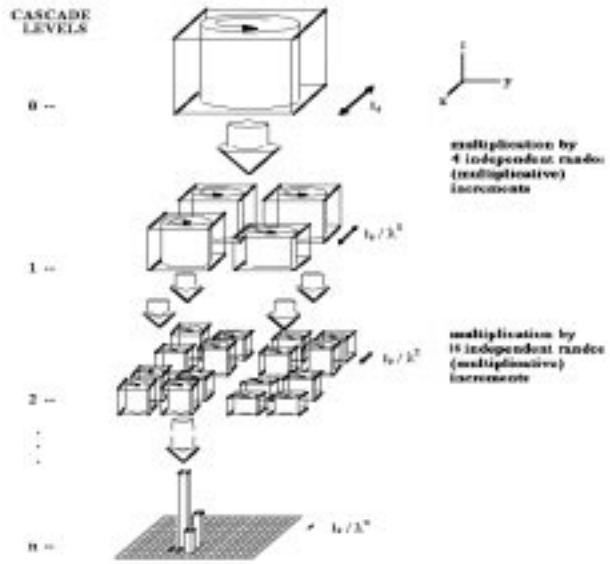

Figure 3: Schematic diagram showing few steps of a discrete multiplicative cascade process.

any intermediate scale ratio λ, e.g. for the scaling function moment $K(q)$:

$$\forall \lambda \in (1, \Lambda) : \ \langle \varepsilon_\lambda^q \rangle \sim \lambda^{K(q)} \tag{4}$$

where the angle brackets indicate ensemble averages and the symbol $\sim$ denotes scaling equality, i.e. the two sides of the equation have the same power law but may have different prefactors, which could be distinct slowly varying functions of the scale ratio Λ.

Generally speaking, for these stochastic multifractal cascades $\varepsilon_\Lambda(\underline{x}, t)$ is defined by an infinite hierarchy of orders of singularity, briefly called singularities, γ. This means that at any scale resolution $\lambda = L/\ell$ (L being the outer scale, ℓ the scale of observation)—this process is scaling:

$$\varepsilon_\lambda \sim \lambda^\gamma \varepsilon_1 \tag{5}$$

$\gamma > 0$ being indeed the algebraic order of divergence of $\varepsilon_\lambda(\underline{x}, t)$; $\lambda \to \infty$, and the frequency of occurrences of a given singularity is governed by the codimension/Cramer function [21,37,61,62]:

$$\Pr(\gamma' \geq \gamma) \sim \lambda^{-c(\gamma)} \tag{6}$$

where "Pr" indicates "probability", γ' is a random singularity and γ is an arbitrary threshold. It is equivalent (by the Mellin transform) to consider the scaling of the different orders q of moments with the associated scaling moment functions $K(q)$ (Eq. 4). In fact, $c(\gamma)$ and $K(q)$ are simply related by the Legendre transform [63]:

$$K(q) = \max_{\gamma}(\gamma q - c(\gamma)); \; c(\gamma) = \max_{q}(\gamma q - K(q)) \tag{7}$$

Note that this codimension multifractal formalism is rather generic for stochastic multifractals and has indeed many advantages [66] compared with the multifractal dimension formalism of deterministic chaos [64]. In particular the codimensions $c(\gamma)$ and singularities γ are intrinsic, whereas the corresponding dimension $f(\alpha)$ and singularities α depend on the dimension D of the space on which the process is observed, this is the reason we label them by a subscript D since we have in general:

$$f_D(\alpha_D) = D - c(\gamma); \; \alpha_D = D - \gamma \tag{8}$$

and similarly:

$$\tau_D(q) = (q-1)D - K(q) \tag{9}$$

Indeed, the main difference between the two formalisms lies in the fact that while the dimension formalism corresponds to enumerating (deterministic) events, the codimension formalism corresponds to defining frequencies of (stochastic) events, i.e. the limit of the ratio of two enumerations, the ratio of the number ($N_\lambda(\gamma)$) of structures with singularities $\gamma' \geq \gamma$ to the total number of structures (N_λ).

$$\Pr(\gamma' \geq \gamma) = \lim_{N_\lambda \longrightarrow \infty} \frac{N_\lambda(\gamma)}{N_\lambda} \tag{10}$$

This limit can be defined even when the determination of $N_\lambda(\gamma)$ is problematic for finite N_λ. When both enumerations are well defined the relationship between dimension and codimension (Eq. 8) is recovered with the help of the heuristic:

$$N_\lambda(\gamma) \sim \lambda^{f_D(\alpha_D)} \; ; \; N_\lambda \sim \lambda^D \tag{11}$$

However, the codimension formalism allows us to explore the interesting cases which are far beyond the applicability of Eq. 8 and has many interesting consequences (see Sec. 2.3) which are missed by the dimension formalism, notably the avoidance of the so-called "paradox of negative/latent dimensions".

Increments of multifractal fields and fractionally integrated fluxes

As mentioned above, the multifractal formalism in turbulence was developed with respect to a scalar measure, the flux of energy, namely its density ε_Λ (in respect to the usual volume measure) which becomes more and more singular at higher and higher resolution ($\Lambda \longrightarrow \infty$). However, directly observable quantities are rather the (vector) velocity field or the temperature field. A classical way [3,15] of analysing these fields, which is rather reminiscent of additive stochastic processes, is to analyse their spatial and/or temporal increments. Note that for the sake of simplicity, we will consider here only spatial processes, the extensions to space-time processes will be discussed in Sec. 4. The statistical moments of the latter are the structure functions, defined by ($\mid \Delta \underline{x} \mid = \frac{L}{\lambda}$) [c]:

$$\langle (\Delta\rho_\lambda)^q \rangle = \langle |\rho_\Lambda(\underline{x} + \Delta\underline{x}) - \rho_\Lambda(\underline{x})|^q \rangle \quad (12)$$

$$\langle (\Delta\rho_\lambda)^q \rangle \sim \langle (\Delta\rho_1)^q \rangle \lambda^{-\zeta_\rho(q)} \quad (13)$$

where the scalar field ρ can be a passive scalar field, the temperature (θ) , or one component of the velocity field (u), the ratio of scale λ, corresponding to the spatial lag is smaller than the resolution of the data Λ ($1 \geq \lambda \geq \Lambda$), $\zeta_\rho(q)$ is the scaling exponent of the structure function.

Dimensional analysis has been widely used to relate the increments of the ρ field to those of a related flux density [d] F:

$$\Delta\rho_\lambda \sim (F_\lambda)^a (\frac{L}{\lambda})^H \quad (14)$$

For $\rho = u$ or $\rho = \theta$, F corresponds respectively to the density of energy flux ε and to a product [21] ϕ of the former with the density of the scalar variance flux χ, the involved powers being derived from dimensional analysis [96,97]:

$$\phi_\lambda = (\chi_\lambda)^{3/2} (\varepsilon_\lambda)^{-1/2} \quad (15)$$

In both cases, again due to dimensional analysis, $a = H = 1/3$. The statistical interrelations between these fluxes will be discussed in Sec. 3, however let us already mention that Eq. 14 implies with the help of Eqs. 7-12 for the scaling moment functions ($K_F(q)$ for the flux F):

$$\zeta_\rho(q) = qH - K_F(aq) \quad (16)$$

[c] Assuming statistical translation invariance, we may omit the location $\underline{x}$ on the r.h.s.

[d] This is a inertial range version of the widely accepted Kolmogorov refined hypothesis [15,16] for the dissipation range.

whereas with the help of Eqs. 6-12 it implies for the singularities (γ_ρ,γ_F being respectively the singularities of ρ and F, with corresponding codimensions c_ρ and c_F):

$$\gamma_\rho = a\gamma - H \ ; \ c_\rho(\gamma_\rho) = c_F(\gamma_F) \tag{17}$$

It is important to note that corresponding to an important property of the basic equations, certain flux densities are conservative (or stationary). As discussed in Sec. 3, it is precisely the case for densities of energy (ε) and scalar variance (χ) fluxes, whereas it is not for their product (ϕ). The "canonical" conservation corresponds to scale independent ensemble averages, i.e.:

$$< F_\lambda >=< F_1 > \iff K_F(1) = 0 \tag{18}$$

The much more demanding "microcanonical" conservation will be discussed in Sec. 2.3. It is also obvious (due to Eq. 16) that in general the increments are necessarily nonconservative, and $H \neq 0$ corresponds to a "mean" degree of non conservation since it is the scaling exponent of the "mean field" increments which could be defined as:

$$< |\Delta\rho_\lambda|^{\frac{1}{a}} >^a \sim \lambda^{-H} \tag{19}$$

Beyond the statistical relationships (Eqs. 16-17), it is rather important to look for a stochastic model corresponding to them. The first - and we argue still the most satisfactory - are the Fractionally Integrated Flux models (FIF) which we discuss below. Others include "synthetic turbulence" [84], the wavelet based approach of Benzi [90], and the bounded cascade model [86]. The first two are rather complicated compared to FIF, but are nevertheless genuine multifractal models. In contrast, the "bounded cascade" (originally developed as an ad hoc model for clouds) is a microcanonical model whose multiplicative factors are algebraically killed off as the cascade proceeds to smaller scales. Although it looks multifractal at large enough scales, the singularities are in fact destroyed resulting in a monofractal small scale limit not very different from fractional Brownian motion. This model lacks a physical basis, and is incompatible with the observed wide range multiscaling statistics of clouds and wind turbulence. For reasons discussed further in Sec. 4, fractionally integrated cascade models [21] have been widely used for defining the field ρ:

$$\rho_\Lambda = I^H(F^a_\Lambda) \tag{20}$$

the fractional integration I^H of order H being defined as a convolution (denoted by $\star$) with a scaling Green's function G:

$$I^H(F_\Lambda^a) = G \star F_\Lambda^a \tag{21}$$

$$D_H \equiv D - H \ : \ G(\underline{x}) \propto \mid \underline{x} \mid^{-D_H} \tag{22}$$

The order of fractional integration H rather corresponds to a codimension, since it is intrinsic to the process (i.e. it does not depend on the dimension D of the embedding space) and is an increment of dimension, and D_H is the associated dimension.

By considering the inverse $G^{(-1)}$, in the sense of convolution, of G (the unity of a convolution algebra being the Dirac function, denoted δ):

$$G^{(-1)} \star G = \delta \tag{23}$$

it is important to note that the filtering induced by the convolution with G (Eq. 21) is equivalent to solving the fractional differential equation defined by $G^{(-1)}$

$$G^{(-1)} \star \rho_\Lambda = F_\Lambda^a \tag{24}$$

This equivalence will be of fundamental importance for the anisotropic (Sec. 2.1) and/or space-time (Sec. 4) extensions, however it is already interesting to note that for the case of isotropic space, $G^{(-1)}$ corresponds to a fractional extension of the Poisson equation, i.e. by denoting Δ the Laplacian:

$$G^{(-1)} = (-\Delta)^{\frac{H}{2}} \tag{25}$$

and G is the corresponding (fractional) Poisson solver.

Most of the previous results are easily derived in the Fourier space, since the Fourier transform of the Green's function satisfying Eq. 22 is:

$$\hat{G}(\underline{k}) \propto \mid \underline{k} \mid^{-H} \tag{26}$$

Finally it is interesting to note that the increments of a fractionally integrated flux have rather distinct behaviors at quite larger or smaller scales with respect to the spatial lag (Appendix A). In comparison, their wavelet transform [87,88] which has become somewhat fashionable [e] in multifractal analysis, is rather trivial since it corresponds merely to convolving the scaling Green's function of the fractional integral with the analyzing wavelet, i.e. to fractionally integrate the latter.

[e] The increments being rather consider as a "poorman's wavelet".

Generalized Scale Invariance (GSI) and Extended Self-Similarity (ESS)

The usual approach to scaling is first to posit (statistical) isotropy and only then scaling, the two together yielding self-similarity. Indeed this approach is so prevalent that the terms scaling and self-similarity are often used interchangeably! Perhaps the best known example is Kolmogorov's hypothesis of "local isotropy" from which he derived the $\frac{2}{3}$ law for the wind fluctuations. Note this had the unfortunate consequence of a priori restricting the relevance of this law to small scales, whereas empirically it applies up to much larger (nonisotropic) scales. In order to overcome this shortcoming, the GSI approach is rather the converse: it first posits scale invariance (scaling), and then studies the remaining non-trivial symmetries. In fact - and this is a common point with Extended Self-Similarity discussed below - one defines a (generalized) scale in a looser way than the usual a priori, academic distance $|\underline{x}|$, (e.g. it does not need to satisfy the triangle inequality), but rather, GSI defines a scale $\|\underline{x}\|$ which is physically defined by the process [f]. For instance, in order to explain the relevance of Kolmogorov law for large scale atmospheric dynamics [75,76,83,89] (see Sec. 4.1 for further discussion), one needs to consider a (generalized) scale defined by a balance between kinetic energy flux (along the horizontal) and buoyancy forces flux (along the vertical). Because of a difference between vertical and horizontal scalings, the balls B_λ defined by this generalized scale

$$B_\lambda(\underline{x}_0) = \{\underline{x}|\ ||\underline{x} - \underline{x}_0|| \leq \frac{L}{\lambda}\} \tag{27}$$

are no longer self-similar spheres, but self-affine balls (e.g. ellipsoids, if B_1 is a sphere or an ellipsoid). Indeed the contraction operator of these balls and of the (generalized) scale:

$$T_\lambda B_{\lambda'} = B_{\Lambda=\lambda\lambda'} \tag{28}$$

$$\|T_\lambda(\underline{x})\| = \lambda^{-1}\|\underline{x}\| \tag{29}$$

is no longer the isotropic self-similar contraction $T_\lambda = \lambda^{-1}\mathbf{1}$, but a self-affine contraction generated by a matrix $\mathcal{G}$ different from the unity:

$$T_\lambda(\underline{x}) = \lambda^{-\mathcal{G}}\underline{x} = e^{-log(\lambda)\mathcal{G}}\underline{x} \tag{30}$$

These rather straightforward geometrical features correspond to important dynamical features of the process. Indeed, using generalized scale notions instead of usual distances in the scaling Green's function (Eq. 22) and the

[f] In a way analogous to that in which the distribution of matter and energy determines the metric in general relativity.

corresponding fractional differential equation (Eq. 24) one obtains self-affine fractional integration/differentiation, i.e. operators involving different orders of integration/differentiation instead of an unique one. In spite of its complexity, such an operator satisfies an unique (generalized) scaling law (similar to Eq. 22):

$$T_\lambda G \sim \lambda^{D_H} G \tag{31}$$

On the other hand, the ratio of the volumes of the balls B_1 and B_λ corresponds to the Jacobian of the transformation T_λ and therefore its scaling yields an effective "elliptical" [g] dimension D_{el}:

$$D_{el} = Trace(\mathcal{G}) \tag{32}$$

$$volume(B_\lambda) = \lambda^{-D_{el}} volume(B_1) \tag{33}$$

Until now, we discuss only the linear and deterministic case of GSI, which will be indeed needed for Sec. 4. However, in order to address the relationship with the notion of Extended Self Similarity (ESS) [90–92], which will be used in Sec. 3, let us first mention that most of the linear GSI features remain for nonlinear and/or stochastic GSI, which, as a one parameter group, is defined by its infinitesimal generator, i.e. by differentiating Eq. 30:

$$\lambda \cdot \frac{\partial T_\lambda}{\partial \lambda} = -\mathcal{G} \cdot \mathcal{T}_\lambda \tag{34}$$

ESS corresponds to considering the scaling in a turbulent cascade not with respect to the usual distance, but with respect to an effective scale defined by the third order moment of the velocity field. As can be inferred from Kolmogorov $\frac{2}{3}$ law (Eq. 1), these two scales are equivalent in the inertial range. This can be argued more rigourously with the help of the (exact) Kolmogorov $\frac{4}{5}$ law [93]:

$$< (\Delta u_\ell)^3 >= \frac{4}{5} \overline{\varepsilon} \ell \tag{35}$$

However, the situation is quite different in the dissipation range, due to the fact the molecular viscosity becomes extremely efficient in damping out the fluctuations. Nevertheless, one may hope that the scale defined by Eq. 35 and which decreases much faster than the usual distance, will be the effective scale on which the scaling properties will be observed, i.e., beyond the inertial range. If this is indeed the case (Sec. 3) this should correspond to a generalized

[g] The term "elliptical" refers to the shape of the balls under GSI transform.

(although isotropic) scale generated by a nonlinear generator. The empirical suppport to ESS, as well as a possible alternative (based on a Lie cascade [109] consideration), are discussed in [106]. One may note that anisotropic ESS has been recently used in order to establish [94,95] a similarity between flows with different geometries (in fact anisotropies), as foreseen in the GSI framework.

Generators of the cascade

Not only is the contraction operator T_λ a one parameter group (Sec. 2.1) but it rescales the one parameter group of the flux density F_λ:

$$F_{\Lambda=\lambda\cdot\lambda'} = F_\lambda \cdot T_\lambda(F_{\lambda'}) \tag{36}$$

which admits also a generator $,_\lambda$ defined as:

$$F_\lambda = e^{\Gamma_\lambda} \tag{37}$$

satisfying the additive property:

$$,_{\Lambda=\lambda\cdot\lambda'} = ,_\lambda + T_\lambda(,_{\lambda'}) \tag{38}$$

In the limit $\lambda \searrow 1$, $,_\lambda$ yields the infinitesimal generator of the group. In a general way, the generator should be thought as resulting from some convolution (e.g. a fractional integration) from a white-noise γ, called the sub-generator of the field [21]. However, due to the fact that the scaling funtion $K(q)$ of the flux F is nothing other than the (Laplace) second characteristic function of its generator [h]:

$$< F_\lambda^q > = < e^{q\Gamma_\lambda} > \tag{39}$$

the generator should have a logarithmic scale divergence in order to satisfy the multiscaling power law (Eq. 4):

$$,_\lambda \sim \log\ \lambda \tag{40}$$

This latter condition restricts the type of integration involved, since considering:

$$,_\lambda = g \star \gamma_\lambda \tag{41}$$

where g is the Green's function for this convolution, and γ_λ is the corresponding white-noise at resolution λ, i.e. independently identically distributed random

[h] It is also called the "cumulant generating function", since the coefficients of its Taylor expansion define the cumulants of the generator.

variables over pixels of the same resolution. Therefore the characteristic function (K_{Γ_λ}) of the generator ($,\ _\lambda$) corresponds to a "path integral" over all pixels (i) of the characteristic function (K_{γ_λ}) of the sub-generator (γ):

$$K_{\Gamma_\lambda}(q) \simeq \sum_i K_{\gamma_\lambda}(qg(\underline{x}_i)) \tag{42}$$

This equation greatly simplifies in the case of an extremely asymmetric and centered Lévy stable sub-generator with a Lévy index α ($0 \leq \alpha \leq 2$) [i], since the (Laplace) second characteristic function of the latter has a scaling behavior (which will correspond to fundamental properties to be discussed in details in Sec. 2.2) :

$$K_{\gamma_\lambda}(q) = c_\alpha q^\alpha \lambda^{-D} \tag{43}$$

where c_α is the singular cumulant of order α. This yields for Eq. 42:

$$K_{\Gamma_\lambda}(q) = c_\alpha q^\alpha \int\limits_{|\underline{x}| \geq \frac{L}{\lambda}} g^\alpha(\underline{x}) d^D\underline{x} \tag{44}$$

Considering a scaling g, i.e. according to Eq. 22, which implies that g^α is of the same type:

$$g^\alpha(\underline{x}) \propto |\ \underline{x}\ |^{-\alpha . D_H} \tag{45}$$

the condition of logarithmic divergence (at small scales) corresponds to a zero dimension of fractional integration for g^α, therefore a corresponding codimension equals to the space dimension D and yields in a rather straightforward manner the adequate order H [21] of g:

$$D_H = \frac{D}{\alpha}\ ;\ H = \frac{D}{\alpha'} \tag{46}$$

where α' is the conjugate of α:

$$\frac{1}{\alpha} + \frac{1}{\alpha'} = 1 \tag{47}$$

Note that extensions of these results to anisotropic cases (thus involving GSI) are trivially obtained by replacing D by D_{el} and $|.|$ by $\|.\|$ in the above equations.

[i] This index α must not be confused with the order of singularity in the dimension formalism (see Sec. 2.1).

Finally, it is important to check that the Fractionaly Integrated Flux model (FIF) is Galilean invariant, not only for theoretical reasons, but also in view of practical applications (in particular for now/fore-casting).

The Galilean transform of a scalar field $X_1(\underline{x}_1, t_1)$ expressed in the Galilean frame $\mathcal{R}_\infty$, into $X_0(\underline{x}_0, t_0)$ in the Galilean frame $\mathcal{R}_\prime$, with $\mathcal{R}_\infty$ having a uniform translation speed $\underline{U}_0$ in respect to $\mathcal{R}_\prime$, corresponds to

$$X_1(\underline{x}_1, t) \;=\; X_0(\underline{x}_0, t) \tag{48}$$

with the Galilean group $\mathcal{U}_{\underline{\mathcal{U}}_\prime}$ transform for the coordinates:

$$(\underline{x}_1, t_1) = \mathcal{U}_{\underline{\mathcal{U}}_\prime}(\underline{\S}_\prime, \sqcup_\prime) = (\underline{\S}_\prime - \underline{\mathcal{U}}_\prime \sqcup_\prime \; ; \sqcup_\prime) \tag{49}$$

Since white noises are statistically Galilean invariant, we need only to consider the Galilean transform of the Green's functions. This is achieved by simply changing the (generalized) scale function $\|.\|_1$ into $\|.\|_0$, according to Eqs. 48-49. The non invariance of the (generalized) scale function $\|.\|$ is due to the fact that the scale contraction operator T_λ does not commute with the Galilean group $\mathcal{U}_{\underline{\mathcal{U}}_\prime}$, therefore is transformed by conjugation with the latter:

$$T_\lambda^{(1)} = \mathcal{U}_{\underline{\mathcal{U}}_\prime} \mathcal{T}_\lambda^{(\prime)} \mathcal{U}_{\underline{\mathcal{U}}_\prime}^{-\infty} \tag{50}$$

2.2 Multifractality and Universality classes

The general framework

Mathematically, an infinite number of parameters is generally necessary to specify a multifractal process. This is because the hierarchy of singularities can have an arbitrary (convex and increasing) codimension/Cramer function $c(\gamma)$ or -equivalently- an arbitrary (convex) scaling moment function $K(q)$. Unless only a few of the infinite number (Fig.4 for illustration) of parameters turn out to be physically relevant, determining the universality classes or basins of attraction (Fig.4 for an illustration), such cascades would be unmanageable either theoretically or empirically. The pioneering claim[17] on log-normal universality in turbulent cascades was shown to be questionable due to the singular small scale limit[40]. More recently, there had been opposite claims[65,67] denying any universality for multifractals. However, even if the singularity of the small scale limit does indeed prevent iterations of the process towards smaller scales from approaching a universal limit, this in no way contradicts the general idea of universality by considering other types of iteration[21,23].

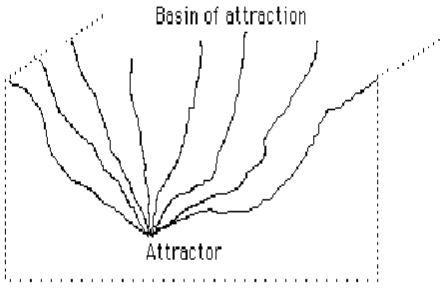

Figure 4: Scheme of a basin of attraction: a stochastic law could depend on as large a number of parameters as the theoretician would like to introduce. Nevertheless, iterations of the corresponding process (e.g. summing identically independent increments for a random walk) could converge to an attractive law depending merely on few relevant parameters (e.g. the "universal" Brownian motion depend on only the finite mean and variance of an elementary step) which define the corresponding basin of attraction.

It was shown [68] that two mechanisms (with possible combination) yield universality: (i) "nonlinear mixing" of these processes: multiplication of independent, identically distributed processes over identical ranges of scales; (ii) "scale densification" of the process: introducing more and more intermediate scales. In both cases, multiplying processes corresponds to adding generators (Sec. 2.1).

Weak and strong universality

Two types of universality [22] can be distinguished: "strong universality" when the generator is stable under renormalization (as displayed on Eq. 43), "weak universality" when the generator and its iterates are only loosely related; they no longer involve stability under rescaling and/or recentering. It seems reasonable that one must seek weak universality only when there is a failure of strong universality. The strong universal scaling functions $K(q)$ and $c(\gamma)$, corresponding to a stable Lévy generator, which process is often called incorrectly "log-Lévy" [j] are:

[j] Let us emphasize that the terms "log-Lévy" or log-normal for the process is rather misleading, because the small scale limit of the latter, as well as its observables obtained by an integration are no longer log-Lévy nor log-normal, due to multifractal phase transitions (sect. 2.3). However, and only for simplicity sake, we will keep this traditionnal terminology.

$$c(\gamma) = C_1 \left(\frac{\gamma}{C_1 \alpha'} + \frac{1}{\alpha} \right)^{\alpha'} ; \qquad K(q) = \frac{C_1}{\alpha - 1} \left(q^{\alpha} - q \right) \tag{51}$$

However, a weak universal multifractal process has been considered [27] yielding "log-Poisson" statistics [28–30]:

$$\begin{aligned} & c(\gamma) = \left(1 - \tfrac{\gamma^+ - \gamma}{c\gamma^-} \left(1 - \log \tfrac{\gamma^+ - \gamma}{c\gamma^-} \right) \right) c \; ; \qquad \gamma \leq \gamma^+ \; ; \\ & c(\gamma) = \infty \; ; \qquad \gamma > \gamma^+ \; ; \end{aligned} \tag{52}$$

$$K(q) = q\gamma^+ + (\lambda_1^{-q\gamma^-} - 1)c \equiv q\gamma^+ - c + \left(1 - \frac{\gamma^+}{c} \right)^q c \tag{53}$$

which turns out to be [22] the classical (and rather trivial) Poisson limit (using a smaller and smaller elementary step $\lambda_{1/N} = \lambda_1^{1/N} \rightarrow 1; \quad N \rightarrow \infty$) of the α-model [42,69,70].

The latter model is the canonical (binomial) model generated by the (Bernoulli) two-state generator γ on elementary discrete step scale ratio λ_1:

$$\begin{aligned} \Pr(\gamma) &= \lambda_1^{-c} \delta_{\gamma - \gamma^+} + (1 - \lambda_1^{-c}) \delta_{\gamma + \gamma^-} \; ; \quad \gamma^+ , \; \gamma^- \geq 0 \; ; \\ \lambda_1^{K(q)} &= \lambda_1^{q\gamma^+ - c} + \lambda_1^{-q\gamma^-} (1 - \lambda_1^{-c}) \end{aligned} \tag{54}$$

γ^+ is the upper bound of singularities; c ($\equiv c(\gamma^+)$) is its codimension and can be chosen rather arbitrarily; γ^- is the lower bound of singularities and is constrained by canonical conservation (Eq. 18). The (monofractal) β-model is recovered for $\gamma^- = \infty$, $\gamma^+ = c = C_1$. Assuming (non-fractal, D=1) filament-like structures (whereas in MHD turbulence one considers extreme events on current sheets [71,72], i.e. D=2) for the highest order singularity and homogeneous eddy turn over times, She and Leveque [27] therefore selected:

$$C = 2, \; \gamma^+ = \frac{2}{3} \; \Rightarrow \; \lambda_1^{\gamma^-} = \frac{3}{2} \; . \tag{55}$$

this choice has some important and questionable consequences for the extreme events (Secs. 2.3 and 3).

On the contrary, the central limit theorem was used to show [68] that the (renormalized) nonlinear mixing of (discrete) α-models leads to a (continuous) "log-normal" multifractal process (i.e. $\alpha = 2$).

2.3 Theoretical and observable bounds on singularities, Self Organized Criticality

For normal and Lévy ($\alpha \geq 1$) generators (the corresponding processes are inaccurately termed log-normal and log-Lévy) there are no bounds on the singularities γ, as is generally the case for canonical processes (Eq. 18). On the contrary, micro-canonical conservation, i.e. per realization of the flux of energy (e.g. the microcanonical version of the α-model called the p-model [44]):

$$\forall \lambda : \int \varepsilon_\lambda d^D \underline{x} = \int \varepsilon_1 d^D \underline{x} \tag{56}$$

not only involves many artificialities [37], but imposes an upper bound: $\gamma \leq D$ (the dimension of space). For $D = 1$, it corresponds to Novikov's celebrated inequality [73] obtained in fact by imposing microcanonical conservation by considering, instead of the energy flux, its dissipation, bounding it by volume integration. The relevance of the dissipation in the inertial range is questionable, especially in the limit of the infinite Reynolds numbers. On the other hand, the necessity of a physical bound to singularities has been argued [74] on the basis of the finite speed of sound. On the contrary, one can consider [75] both incompressible Navier-Stokes equations (without any characteristic velocity, infinite speeds of sound) and the physical issues of compressible turbulence involving compressibility effects. The corresponding hypersonic gradients are of course beyond the scope of incompressible Navier-Stokes equations. It can be argued [75,77,23] that not only do unbounded singularities pose interesting problems of observation and estimation, but are a requisite to the introduction, via first order multifractal phase transitions, of a non classical Self- Organized Criticality [78,79] (SOC), which is often desirable in order to explain the phenomenology of extreme events. For SOC singularities, the observed singularities (empirically bounded by γ_s, the maximum reachable singularity (see below) in the samples studied) has a codimension different from the theoretical one given by Eq. 6:

$$c(\gamma) = q_D \gamma - K(q_D) \; ; \quad \gamma_s \geq \gamma \geq \gamma_D = K'(q_D) \tag{57}$$

where γ_D is the critical singularity of transition to SOC. Therefore, the observed codimension for SOC singularities ($\gamma_s \geq \gamma \geq \gamma_D$) follows the tangent instead of the theoretical parabola-like codimension, which means that the probability distribution of these extreme events has an algebraic fall-off. Consequently there is a divergence of higher order moments $q \geq q_D$ for infinite samples. However, the finite size of empirical datasets impose the bound γ_s,

and with this condition the Legendre transform of Eq. 57 yields the following estimated $K(q)$:

$$K(q) = \gamma_s q - c(\gamma_s); \quad q \geq q_D \tag{58}$$

i.e. is also linear in q, of slope γ_s. One may note that we have:

$$\gamma_s - \gamma_D = \frac{c(\gamma_s) - c(\gamma_D)}{q_D} \tag{59}$$

When the number of samples increases, $\gamma_s \rightarrow \infty$ which corresponds to divergence of higher moments. More precisely, the number N_s of the sample scales as $N_s \simeq \lambda^{D_s}$ (at the resolution λ), where the exponent D_s is the "sampling dimension" can be estimated:

$$c(\gamma_s) = D + D_s \equiv \Delta_s \tag{60}$$

γ_s is the highest singularity almost present in the sample and Δ_s is the overall effective dimension of the sample. The fact that $c(\gamma_s) > D$ is the origin of the paradox of negative/latent dimension of the dimension formalism which we already mentionned.

One must note that ironically the α-model was developed to illustrate the generality of divergence of moments for multifractal fields, which is obtained as soon as its basic parameter q_D (originally denoted α):

$$q_D \simeq (c - D)/(\gamma^+ - D) \tag{61}$$

is greater than 1, which correspond to $c > \gamma^+ > D$. However the parameters (Eq. 55) chosen by She and Leveque[27] for the canonical $\alpha-$model/log-Poisson model do not satisfy these conditions and therefore do not yield SOC like all microcanonical multifractal processes (Eq. 56).

2.4 Double Trace Moment (DTM) and normalized powers of a multifractal field

A striking feature of universal mulitfractals is that their scaling functions (Eq. 58) are non analytical at $q = 0$, with the only exception: $\alpha = 2$. The Double Trace Moment[80–82] technique (DTM) – which corresponds to raising the data (at the highest resolution), to the power η, then to estimating the scaling of the corresponding (trace-) moments computed at various degraded resolutions– has been widely used to test[25] the non analyticity of $K(q)$ ($\alpha < 2$) at $q = 0$. In fact, this technique corresponds to estimating the scaling function

$K(q,\eta)$ (similar to $K(q)$, Eq. 4, $K(q,1) \equiv K(q)$) of the normalized η power of the field [77]:

$$\varepsilon_\lambda^{(\eta)} = \frac{\varepsilon_\lambda^\eta}{\langle \varepsilon_\lambda^\eta \rangle} \tag{62}$$

therefore:

$$K(q,\eta) = K(\eta q) - qK(\eta) \tag{63}$$

which obviously has the same type of analyticity as $K(q)$. Indeed, for (strong) universal multifractals:

$$K(q,\eta) = \eta^\alpha K(q) \tag{64}$$

The corresponding codimension function to $K(q,\eta)$, i.e. the scaling exponent function of the corresponding probability distribution of the singularities γ of the field:

$$\varepsilon_\lambda^{(\eta)} \sim \lambda^{\gamma'} \; ; \; Pr(\gamma' \geq \gamma) \sim \lambda^{-c(\gamma,\eta)} \tag{65}$$

is:

$$c(\gamma,\eta) = c(\frac{\gamma + K(\eta)}{\eta}) \tag{66}$$

$K(q,\eta), c(\gamma,\eta)$ are, as $K(q), c(\gamma)$, dual for the Legendre transform. The critical singularities γ_s and γ_D, discussed in sect. 2.3 generalized into $\gamma_s^{(\eta)}$ and $\gamma_D^{(\eta)}$, corresponding (for any given η) respectively to the maximum observable singularity due to the finite size of sample (finite Δ_s in Eq. 60) and the (finite) critical order of statistical divergence for higher order moments. They define in the plane (η, q) two critical curves of "multifractal phase transitions" [77], respectively of second ($q_s^{(\eta)}$) and first order($q_D^{(\eta)}$). In the case of universal multifractals, we have:

$$c(\frac{\gamma_s^{(\eta)}}{\eta^\alpha}) = \frac{\Delta_s}{\eta^\alpha} \tag{67}$$

$$q_s^{(\eta)} = (\frac{\Delta_s}{C_1 \eta^\alpha})^{\frac{1}{\alpha}} \tag{68}$$

$$K(q_D^{(\eta)}) = \frac{D}{\eta^\alpha}(q_D^{(\eta)} - 1) \tag{69}$$

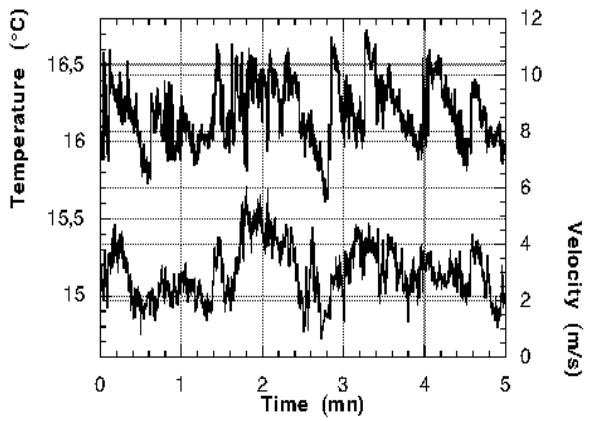

Figure 5: A sample of simultaneous velocity and temperature data, showing intermittencies at all scales.

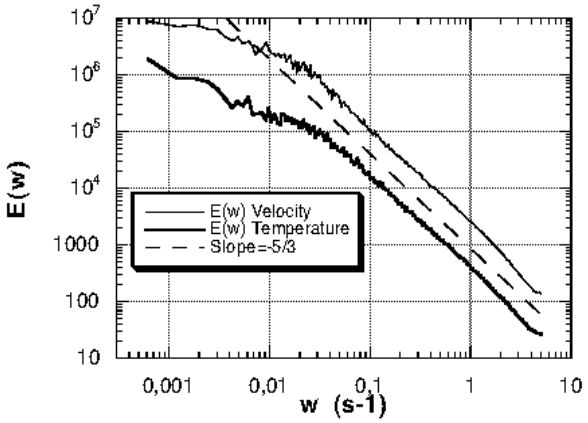

Figure 6: The Fourier power spectrum of the velocity and temperature data, in log-log plot, showing a power-laws for more than 2 decades, with slopes of $\beta \sim 1.70$ for velocity and $\beta \sim 1.62$ for temperature; a dotted straight line of slope $-5/3 \sim -1.67$ is shown for comparison.

3 Velocity and temperature turbulence: scaling exponents for intermediate, weak and extreme events

The traditionnal way of testing the validity of scale invariant models in turbulence is to compare empirical estimates of the structure function (Eq. 12) scaling exponents (Eq. 13) to theoretical values corresponding to different models (e.g. strong or weak universality, Sec. 2.2). These models generally have one to three free parameters, which are then determined using theoretical justifications or empirically.

As we discuss below, it turns out that there are mainly three qualitatively different ranges of singularities:

- *Intermediate range.* Velocity structure functions up to moment of order 7 can be empirically estimated and compared to log-Poisson and "log-Lévy" models; this corresponds to considering intermediate orders of singularities. Indeed, as shown recently by an unsuccessful collective attempt to reach (artificially) a consensus [99], clear agreement can only be obtained up to moments of order 7.

- *Low range.* We can also focus on low orders of singularities, associated with moments of orders near 0; in this way, we investigate possible non-analyticity predicted by the "log-Lévy" model 2.4. This is a direct test capable of simply distinguishing strong universality from other models.

- *High range.* We finally consider high order singularities, associated with moments of order larger than 7; this is another direct way of testing the log-Poisson model which rests on an assumption of a fixed largest order of singularity, whereas the "log-Lévy" model has no upper bound and therefore leads to multifractal phase transitions (Sec. 2.3). This implies that the values of the large orders of moments will depend on the number of realizations studied in the sample.

3.1 Intermediate order singularity analysis

The data and their spectra

We consider here time series of velocity ($\rho = u$) and temperature measurements ($\rho = \theta$) recorded with a sonic anenometer located 25 m above ground, over a pine forest in south-west France, sampling at $\omega_s = 10Hz$ (see [103] for a presentation of the dataset). We analyzed 22 profiles of duration 55 minutes each. Samples of the velocity and temperature data are shown in Fig. 5. They clearly show a huge intermittency, with fluctuations at all scales.

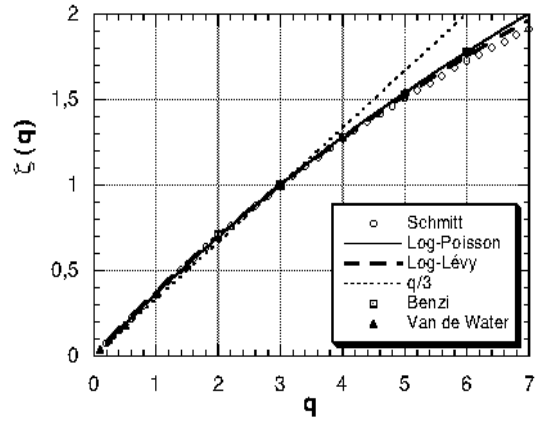

Figure 7: Empirical values of the structure function scaling exponent $\zeta_V(q)$ for the velocity field compared to log-Poisson and log-Lévy models. Up to moments of order 7 the two models provide excellent fits and cannot be discriminated.

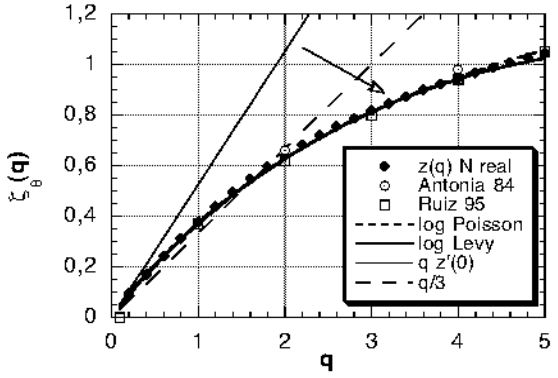

Figure 8: Our estimates of $\zeta_\theta(q)$ plotted vs. q, for moments up to 5. Also shown for comparison the values reported in other studies: all the empirical data we report here are very close to each other. The thin continuous lines correspond to the theoretical models proposed in the text: this shows that the fits are very good, and that each of these two models can be considered to be compatible with the data for $q \leq 5$.

The energy associated with each scale is given by the power spectra, which within the inertial range follow a scaling behavior:

$$E(\omega) \sim \omega^{-\beta} \tag{70}$$

over frequencies from about $\omega_s/1000$ to $\omega_s/2$ (see Fig. 6 for the two spectra). β is the exponent of the scaling of the power spectra. We obtain for the velocity data $\beta_u \simeq 1.7$, which is not far from the Kolmogorov 5/3 value[3]. The slight difference with the exact 5/3 value is usually attributed to intermittency effects, as discussed in the next section. For the temperature data, we obtain $\beta_\theta \simeq 1.62$, which is less steep than the 5/3 value which would be obtained in the case of homogeneous Obukhov-Corrsin turbulence [96,97]. This is in agreement with the value reported in [100], and shows that the "intermittency correction" to the famous "5/3 law" for temperature is of opposite sign as for the velocity.

Structure functions: general case

We recall that dimensional analysis has been used to relate the increments of the ρ field (u or θ) to those of a flux F_λ. This yields Eq. 14 and by consequence a linear relationship (Eq. 16) between the structure function scaling exponent: ζ_ρ and the scaling function of the flux K_F and H, the latter corresponds at the same time to a "mean degree of conservation" (Eq. 19) and to the order of the corresponding fractionally integrated cascade model (Eq. 21) .

Velocity structure functions

For velocity turbulence, F is the energy flux density ε and is usually assumed to be a canonically conservative, i.e. $K_\varepsilon(1) = 0$ (Eq. 18). The parameter values $H = a = 1/3$, obtained by dimensional analysis, give a third order moment of the velocity structure function: $\zeta_V(3) = 1$ in agreement with the Kolmogorov $\frac{4}{5}$ law (Eq. 35). Therefore, $\zeta_V(q)$ (Eq. 16) depends only on the form of $K_\varepsilon(q)$, which has different analytic expressions for the different cascade models: see Eq. 51 for the log-Lévy model and Eq. 53 for the log-Poisson model.

We here first test these different universal models directly using the structure functions. For better precision their scaling exponents $\zeta_V(q)$ were estimated [22] with the help of extended self-similarity techniques [90–92] (ESS, see discussion above). Furthermore, the use of absolute values in Eq. 12 allows one to obtain a (near) continuous empirical curve for $\zeta_V(q)$ whereas other works [27,29,30] estimate only the first 10 integer moments. Fig. 7 displays our empirical estimates of $\zeta(q); q \in (0,7)$, the empirical values of Benzi et al. [92], those of Van de Water [99], as well as the theoretical estimates of the log-Lévy

(with $\alpha = 1.5$ and $C_1 = K'(1) = 1 - 3\zeta'(3) = 0.15$ for Eqs. 51 and 16, see [22]) and log-Poisson (with $c = 2$ and $\gamma^+ = 2/3$ for Eqs. 53 and 16, see [27]) models. We see that the different experimental estimates are in very good agreement with each other, and that the two models we test (with the values of the parameters given above) are in excellent agreement with experimental estimates, and therefore cannot be directly discriminated.

This is nevertheless an important achievement, since for now, up to moment of order 7, several teams agree on the empirical values of scaling exponents of velocity structure functions. This can be used, for example, to determine the free parameters in the competing multiplicative models.

Temperature structure functions

For temperature structure functions, dimensional arguments still give Obukhov-Corrsin law [96,97], i.e. $H = a = 1/3$, however the flux $F = \phi$ (Eq. 15) involves not only the conserved energy flux ε_λ, but also the conserved scalar variance flux $\chi_\lambda \sim \frac{\lambda}{L}(\Delta\theta_\lambda)^2 \Delta u_\lambda$. It is not necessarily conserved, and its moments have no known simple expression in the general case. Some asumptions have to be made for the correlations (e.g. between ϵ and χ or ε and $\Delta\theta$, see [105,106] for more details).

- A simple but rather unrealistic hypothesis would be to consider that the fluxes ε and χ are completely correlated [21]. This leads to much simplification:

$$K_F(q) = K_\varepsilon(q) = K_\chi(q); \;\; \zeta_\theta(q) = \zeta_u(q) \tag{71}$$

- The opposite extreme hypothesis [107], corresponds to ε and χ are completely independent. In this case, the characteristic functions add, and we obtain (see also [105]):

$$K_F(q) = K_\chi(3q/2) + K_\varepsilon(-q/2); \;\; \zeta_\theta(q) = q/3 - K_F(q/3) \tag{72}$$

  This hypothesis is obviously much more unrealistic, due to the fact that the velocity field advects the scalar field, so the two fluxes are likely to be at least somewhat correlated. The negative power in ε is also a problem [105] for low values of the wind shear, which may render $K_\varepsilon(-q/2)$ divergent (this is the case if ε is a strong universal multifractal with $0 < \alpha < 2$).

- The correct hypothesis is obviously between the two. Here, the precise hypothesis we follow in [105] is an hypothesis of independence of the increments $\Delta\theta$ and Δu (not of the fields themselves, which are certainly

correlated). It has some theoretical grounds [104] and yields the following expression:

$$K_F(q) = K_\chi(3q/2) - K_\varepsilon(q/2); \;\; \zeta_\theta(q) = q/3 - K_F(q/3) \qquad (73)$$

This was shown to be empirically verified [105] up to moment of order about 6.

In this latter case, we argued [106] that, due to the fact that nonlinear mixing (Sec. 2.2) of multifractal processes lead to universality[k], the fluxes ε and χ belong to the same universality class (i.e. the same value of α), as well as the flux ϕ. Eq. 73 then yields:

$$C_{1F} = (3/2)^\alpha C_{1\chi} - (1/2)^\alpha C_{1\varepsilon} \qquad (74)$$

We empirically obtain $\alpha_\varepsilon \simeq 1.5 \pm 0.1$ and $\alpha_\chi \simeq 1.4 \pm 0.1$, which is compatible with $\alpha \simeq 1.45 \pm 0.15$ and (using $C_{1\varepsilon} \simeq 0.16 \pm 0.02$, $C_{1\chi} \simeq 0.22 \pm 0.02$) $C_{1F} \simeq 0.34 \pm 0.04$ (see [106]), the flux ϕ is not conserved, because $K_\phi(1) = K_\chi(3/2) - K_\varepsilon(1/2) \simeq 0.19 \pm .02 \neq 0$.

On the contrary, the log-Poisson model is not strongly universal and therefore is not stable under nonlinear mixing. Indeed the form of $K(q)$ in Eq. 53 is not closed under linear combination as given by Eq. 73. As a result, we see that it is rather impossible for temperature turbulence to have log-Poisson statistics in the case where the two fluxes ε and χ do have log-Poisson statistics. Nevertheless, we empirically test the proposal of Ruiz Chavarria et al. [101] who merely assumed that the temperature fluctuations follow a log-Poisson law (see Eq. 53) for $\zeta_\theta(q) = q\zeta_\theta(1) - K(q)$, without considering the problem of the nonlinear product between two fluxes (Eq. 15). They proposed on empirical grounds the following values: $\zeta_\theta(1) \simeq 0.37 \pm 0.02$; $\gamma^+ \simeq 0.31$; $c \simeq 0.84 \pm 0.1$.

For precise empirical estimates of $\zeta_\theta(q)$, we used the ESS, as in [100,101]. Fig. 8 displays the resulting function $\zeta_\theta(q)$, for moments up to order 5 (with a 0.1 increment). For comparison, the empirical results [100,102] are plotted on the same figure.

The very good correspondence observed in this figure indicates that the two universal models with the above parameters are compatible with the data through the medium range of moments ($q \leq 5$). Despite the incompatibility of the log-Poisson assumption for velocity and at the same time for temperature (they can hardly simultaneously have log-Poisson statistics), we use below more sensitive techniques in order to discriminate log-Poisson and log-Lévy models, using methods dealing with low order singularities.

[k] In the case of passive advection, it indeed corresponds to the original "test field" argument [37].

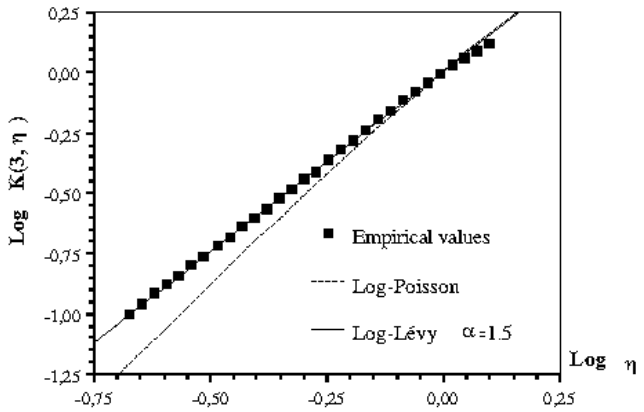

Figure 9: Double trace moment estimate of the energy flux: $K(3,\eta)$ vs. η in a log-log plot, where $K(q,\eta) = K(q\eta) - qK(\eta)$. The log-Poisson model yields a slope (=α) of 2 (due to analyticity), whereas empirical values yield $\alpha \simeq 1.5$.

3.2 Low order singularity analysis

General case

In order to better discriminate the models, we must use analysis techniques directly dealing with the nonlinearity of the $\zeta(q)$ curve. This is done using two different methods.

The first one is the DTM technique (Sec. 2.4), which can be applied to a positive multifractal flux. The non-conservative data (if $\zeta(1) \neq 0$) must then be transformed through a fractional derivative before applying the DTM (see [25]).

The second method involves analysis of the function $f(q) = q\zeta'(0) - \zeta(q)$ (see [108]); note that finite difference approximates are often adequate. We have already discussed (Sec. 2.4) the fact that $K(q)$, $K(q,\eta)$, $\zeta(q)$, and other related quantities (such as $f(q)$ when $\alpha > 1$), are non-analytical at $q = 0$. In general (when $\alpha \neq 2$) this latter quantity is precisely (as $K(q,\eta)$) a non-integer power law. This can be seen using the following expressions:

$$\zeta(q) = qH - K_F(aq) = q\zeta(1) - a^\alpha K_F(q) \quad (75)$$

$$\zeta'(0) = \zeta(1) + a^\alpha \frac{C_{1F}}{\alpha - 1} \quad (76)$$

$$f(q) \quad = \quad q\zeta^{'}(0) - \zeta(q) = a^{\alpha}\frac{C_{1F}}{\alpha - 1}q^{\alpha} \tag{77}$$

Therefore, in a log-log plot, $f(q)$ vs. q should display a slope of α.

These methods are useful in order to directly determine the main multifractal parameter, α. The value of C_{1F} is then only a multiplicative constant which is much easier to determine. These analysis techniques help to discriminate between different universal models. They show the relevance of the log-Lévy model for the low and intermediate orders of singularities.

Low order singularity analysis for velocity data

The velocity data have been transformed into energy flux through a fractional differentiation (for details see [25]). The DTM technique is then applied: this is applied in Fig. 10; it clearly shows that log-Lévy universality is closer to the data than log-Poisson, especially for low order singularities.

We also applied the "$f(q)$ technique" directly on the velocity data. The result is shown on Fig. 9: it clearly yields $\alpha \simeq 1.5$ instead of α=2 for the log-Poisson model and α-model (see theoretical curves). In Sec. 5, we also show that similar values for α are obtained from numerical simulations of SGC, which could be considered as Navier-Stokes caricatures.

Low order singularity analysis for temperature data

As for the velocity case, we intend to discriminate the models using another analysis technique. The DTM technique is not applied here because the corresponding flux is not simple, as shown above.

Also shown in Fig. 8 are respectively the homogeneous Obukhov-Corrsin case ($\zeta_\theta(q) = q/3$), and the tangency at $q = 0$ ($\zeta_\theta(q) = q\zeta_\theta^{'}(0)$) with $\zeta_\theta^{'}(0) \simeq 0.53$. Using this latter estimate, Fig. 11 displays a log-log plot of $f(q)$ vs. q. The thick and straight line corresponds to the universal model with $\alpha = 1.45$, which fits the data rather well, although there is a discrepancy for very low order of moments/singularities, which is presumably due to the sensitivity limitation of the the measuring sensor. The dotted line represents the log-Poisson model. One may note that the deviation between the two models will be clearer as soon as one explores sufficiently low orders of moments: since we consider shears, this requires storing data using more digits (larger dynamical range).

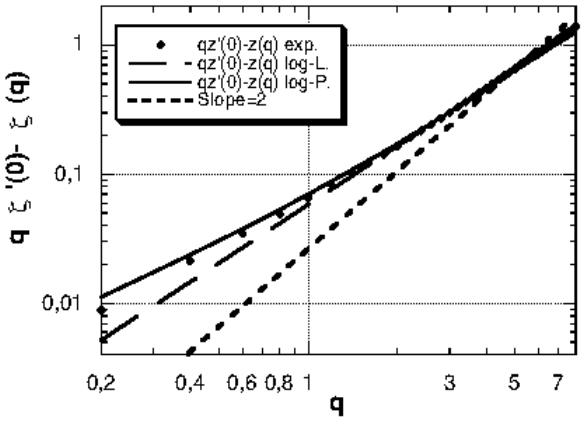

Figure 10: A direct test of the non-analyticity of the velocity data, using the $f(q)$ function (see text). The data are compatible with the log-Lévy model, showing non-analyticity, and at the same time are not compatible with log-Poisson model for weaker events, because the latter is analytic.

3.3 High order singularity analysis

General case

The main physical feature of the log-Poisson model is in fact an hypothesis of a fixed maximum singularity. Because it is universally fixed, this maximum singularity should be the same for any number of realizations: it should be reached already for one realization; it should also not depend on the sampling, and be stable even if the number of realizations increases.

In order to check this, we studied the influence of the number of realizations, i.e. we decomposed our data series into 704 different portions of length 512 datapoints each, because the maximum scale ratio for the scaling range is about 500. First, we considered the estimation of $\zeta(q)$ for one realization: for this, for each portion i of the dataset, we estimate one $\zeta^i(q)$. We then take the mean of all these exponents $\zeta^i(q)$ as being $\zeta_1(q)$, the scale invariant function for one realization:

$$\zeta_1(q) = \frac{1}{704} \sum_{i=1,704} \zeta^i(q) \tag{78}$$

For 704 realizations, we evaluate $\zeta_{704}(q)$ using an ensemble average for all

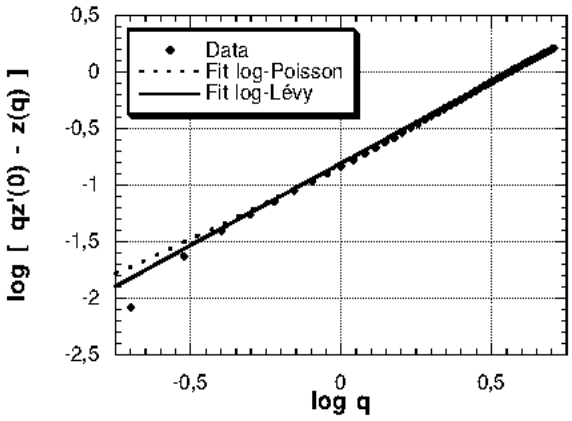

Figure 11: The non-analyticity tested on the temperature data, compared to the two models studied here, in log-log (decimal log) plots. A straight line of slope smaller than 2 is an indication of non-analyticity, and thus a confirmation of the validity of the log-Lévy model.

the realizations [l]. In case of a first order multifractal phase transition (see Sec. 2.3), associated to a divergence of moments at $q = q_D$, we have the following behavior for $\zeta(q)$:

$$\zeta_{704}(q) = \zeta_1(q) \; ; \; q < q_D \tag{79}$$

$$\zeta_N(q) = c(\gamma_N) - \gamma_N q \; ; \; q \geq q_D \tag{80}$$

where γ_N is the maximum singularity reached for N realizations. When N increases, the slope $-\gamma_N$ of the straight line for $q \geq q_D$ decreases, and the intercept $c(\gamma_N)$ increases.

Therefore, as shown in [10,3,22], a study of the large q asymptote of $\zeta(q)$ for 1 and 704 realization is a way to directly detect the divergence of moments and quantitatively estimate its order.

High order singularity analysis for velocity data

In Fig. 12 we apply the method described above to velocity data. The linear asymptote for 1 realization has the equation $\zeta_1(q) = 0.205q + 0.5$, for $q \geq 7$.

[l] Let us note the distinction: $\zeta_{704}(q)$ is obtained through a log-log plot of the ensemble average of all the values of the moments, whereas $\zeta_1(q)$ is the mean of all the values obtained through a log-log plot of the moments for each realization.

We see also that the estimates for 1 and 704 realizations deviate significantly from each other for moments order $q \geq q_D \simeq 7 \pm 0.5$ and that for these values $\zeta(q)$ is linear as predicted by Eq. 80 (with $\gamma_{s,u} = -0.205$ and -0.124 and $c(\gamma_{s,u}) = 0.5$ and 1.11 for 1 and 704 realizations respectively). We may note that in the log-Poisson model there is also a linear asymptote: $\zeta(q) = \frac{1}{9}q + 2$. This behavior is clearly not compatible with our data: for 1 realization, the asymptotic slope is too large, and if we increase the number of realizations, it decreases, becoming smaller than $\frac{1}{9}$. This would have been more obvious if we had more realizations, but even here for 704 realizations the intercept of the asymptote is clearly too small to be compatible with log-Poisson extreme events.

We finally note that the critical moment $q_D = 7. \pm 0.5$ of the order of divergence of moments was previously estimated with different methods [103]. As was done in [103], we predict here that all structure function scaling exponents are linear for moments larger than this critical value, with a slope which decreases with the number of realizations as more and more SOC structures are analyzed (see [83] for meteorological implications). This seems to be implicitly confirmed by the "consensus paper" [99] where the only agreement obtained between different researchers for turbulence structure functions was the value of $\zeta(q)$ up to order 7. The different teams involved in this paper had different numbers of realization in their data sets, giving different values for the asymptote, easily explaining why a "consensus" cannot be reached for a universal and definitive value for the empirical asymptote of $\zeta(q)$.

High order singularity analysis for temperature data

As done for the velocity, we study the temperature structure functions for 1 and 704 realizations. This is shown in Fig. 13. For moments larger than 5 the empirical values become linear, with an asymptote whose slope decreases with the number of realizations. For one realization we obtain $\zeta_1(q) = 0.11q + 0.68$. When 704 realizations are used, the linear asymptote has the equation $\zeta_{704}(q) = 0.06q + 0.78$, for $q \geq 5$. One may note that is not far from the empirical asymptote $0.06q + 0.84$ proposed in [101]. But this does not mean that the log-Poisson is confirmed: these values were fitted in [101] using their empirical asymptote, which happens to be roughly the same as ours (because we had roughly the same number of realizations as they did). However, the log-Poisson model assumes that this asymptote is already reached for one realization, whereas we just saw that this is not the case. This change of the slope and intercept of the asymptote with the number of realizations is therefore another strong piece of evidence against the log-Poisson model. Even if we

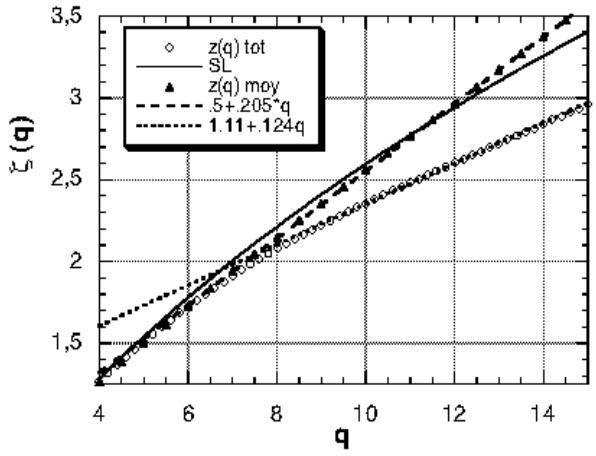

Figure 12: The asymptotic behavior of the scale invariant moment function for the velocity field, for 1 and 704 realizations, compared to the log-Poisson model. We may note that an empirical departure from the "bare" log-Lévy model is expected, because observables are associated to multifractal phase transitions. This arises here at the moment of order 7.

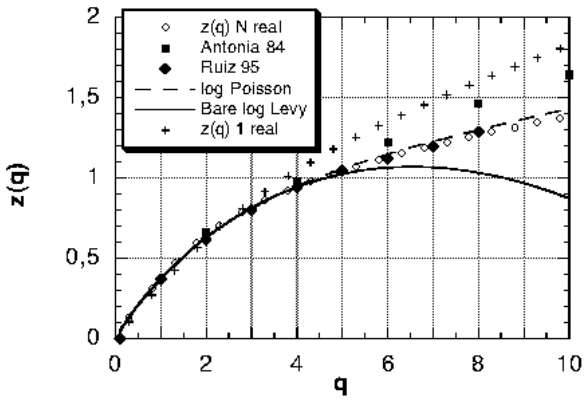

Figure 13: The asymptotic behavior of the scale invariant moment function for the temperature field, for 1 and 704 realizations, compared to the two models studied here. As for the velocity data, we oberve a first order multifractal phase transitions at the moment of order 5: for larger moments, an asymptotic straight line is reached, with a slope depending on the number of realizations.

did not find it here, we can infer that with a larger dataset one obtains an asymptotic slope smaller than that proposed in [101].

We may note finally that the value of q_D for temperature fluctuations is smaller than for velocity. The consensus on empirical values of $\zeta_\theta(q)$ should therefore be restricted to lower moments than for velocity.

4 Causal space-time multifractals

4.1 General considerations

A general feature of turbulence is that for structures with given size ℓ, there is a typical lifetime (e.g. "eddy turn-over time") τ_ℓ, related dimensionally by the shear velocity (see below). In such system, and notably for atmospheric turbulence, the velocity itself is scaling over much of the dynamically significant distances, and one is immediately led to a space-time scaling model in which space-time is stratified due to the scale dependence of the velocity, while a scale independent velocity, the original Taylor's hypothesis of frozen turbulence [123], would yield isotropic space-time. This space-time model is quite at odds with the usual meteorological phenomenology which posits on purely phenomelogical grounds a whole hierarchy of qualitatively different dynamical (highly scale dependent) mechanisms. Fig. 14 illustrates this with a reproduction of the standard view of the atmosphere indicating the typical lifetimes and sizes of various atmospheric phenomena. This figure - or close variants - can be found in almost all introductory meteorological texts. Indeed, so different is this from the scaling approach discussed here, that at first sight, it is not obvious how the two can be reconciled. However, it is easy to see that this schematic is not only compatible with scale invariance, but even demands it! The reason is that the phenomena all lie along a diagonal on the log-log plot indicating that the lifetime/size relation is a power-law; that the law has no characteristic size (in this scale invariant view, the spread of values about the straight line is simply a manifestation of intermittency, stochasticity). Better still: the slope is very close to the (Kolmogorov) value of 2/3 which is theoretically predicted using cascade processes and dimensional analysis (see below). In short, a priori, it is sufficient to simply drop the ad hoc supposition that differences in appearance correspond to qualitative dynamical differences. This alternative view, the "unified scaling" model [76,47], of the atmosphere involving anisotropic but scaling multifractal cascades, is indeed the only one compatible with these observations, especially within the "meso scale" range (around 10 km, the scale corresponding roughly to the "thickness" of the atmosphere).

In turbulence, experimental methods for measuring the intermittency are

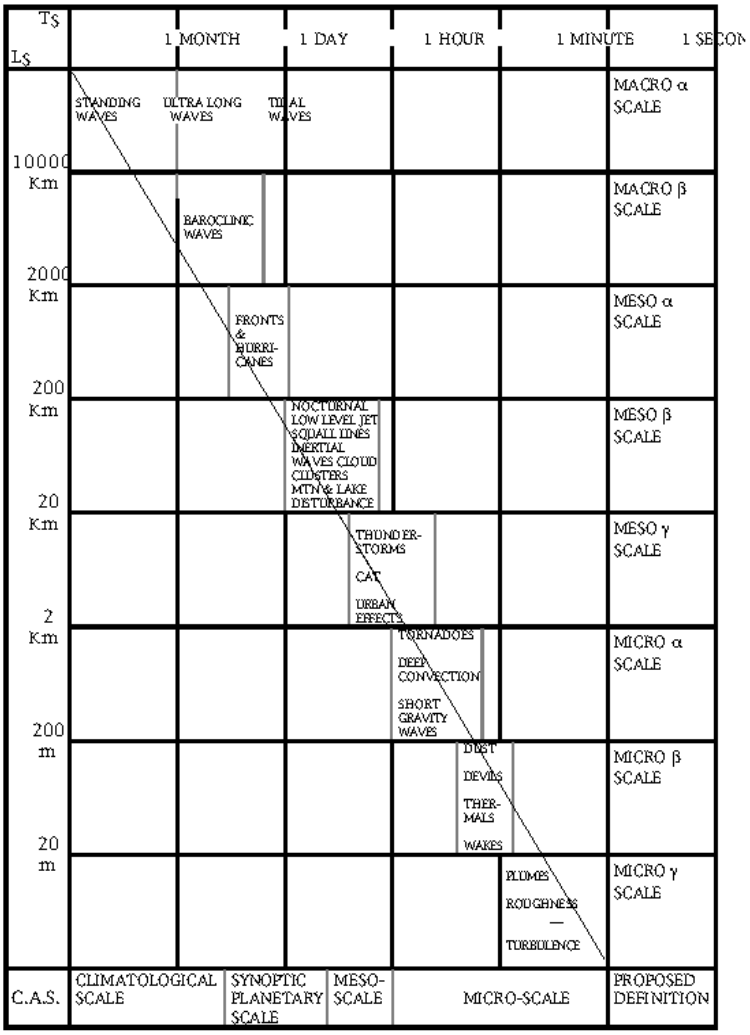

Figure 14: Schematic diagram showing a typical phenomenologist's view of meteorology (reproduced from Atkinson[121] who adapted it from Orlanski[122]. The straight line, added by the authors, is the Kolmogorov scaling $\tau_\ell \sim \ell^{2/3}$ where we have made the interpretation that the lower right corner of the inner frame is 2 m and 10 s, whereas the upper left intersection of the inner frame with the extension of the line corresponds to one month.

mostly based on 1-D time series; thus purely spatial and purely temporal properties are very rarely analyzed all together. Instead, they are usually linked through Taylor's hypothesis. Historically, a very different approach was needed for rainfall fields; such fields have been shown to respect scaling symmetries, on wide ranges of scales [124], perhaps from 10^{-3} m to $10^6 - 10^7$ m. Although rain is certainly far from being simply a passive scalar advected by the atmospheric turbulence it may nevertheless respect the same cascade phenomenology. Indeed, the use of radar data (1-D time series of 1 to 3-D spatial scans), and the statistical link between radar reflectivity and rainfall intensity, have given an original view on the relationship between spatial and temporal properties of the cascades. Quite naturally, Taylor's hypothesis was questionned [132,125,133,124,26]; more precise assessments of the dynamics of the spatial cascade had to be investigated.

Recently, two models have been proposed for rainfall (Over et al. [126] and Marsan et al.[51] for rainfall and turbulence), while another model[127] was dealing with turbulence, all going beyond the simple Taylor's hypothesis. However, the models proposed in [126,127] are based on Markovian Lagrangian dynamics; this is in contradiction with the fact that the Navier-Stokes equations possess scaling symmetries along both the spatial and the temporal axis (a property that is expected to hold for rainfall). Building directly on these symmetries, the model described in [51](see also Brenier et al. [50] for a similar but non-causal approach) is a natural extention of traditionnal cascade models, classically defined on a spatial domain, to space-time domains, taking into account both the scaling anisotropy between space and time (accordingly to the Kolmogorov-Obukhov theory, for turbulence) and the breaking of the mirror symmetry along the temporal axis, i.e., causality. Note that, similarly, the SGC model detailed in Sec. 5 (see also [52]) leads also to multiscaling in both space and time.

In this section, we will consider the space-time extension of fractionally integrated flux models, and study both their predictability limits and their forecasting capacity.

4.2 Causal cascade models

Space-time anisotropy

As explained in Sec. 2.1, cascade models operate through a scale-invariant generator acting from the largest scale L down to the smallest scale $l = \frac{L}{\Lambda}$ of the system, Λ being the maximum resolution or scale-ratio, thus creating structures at all scales.

These structures created at all scales $\ell \in [l; L]$ are interpreted as typical eddies transfering energy to smaller scales through a shearing process; such

eddies possess a life-time τ_ℓ depending on ℓ, after which they are considered to have been swept by other structures. In the framework of homogeneous turbulence [3,4], this life-time is a characteristic time for each scale, and scales like:

$$\tau_\ell \ \sim \ \ell^{\frac{2}{3}} \bar{\epsilon}^{-1/3} \tag{81}$$

with $\bar{\epsilon}$ being homogeneous in space and in scale. For inhomogeneous turbulence [15,16], the same scaling relation should hold only on the average, whereas at any given scale ℓ, the eddy turn-over time τ_ℓ is spatially intermittent, and depends on the non-homogeneous ϵ_ℓ rather than on $\bar{\epsilon}$.

In the (D + 1-dimensional) space (D-dimensional)-time (1-dimensional) domain, Eq. 30 becomes

$$T_\lambda : (\underline{x}, t) \rightarrow \lambda^{-\mathcal{G}} (\underline{x}, t) \tag{82}$$

The Kolmogorov-Obukhov theory leads to choosing the matrix $\mathcal{G}$ as

$$\mathcal{G} = \begin{pmatrix} 1_D & 0 \\ 0 & 1 - H_t \end{pmatrix} \tag{83}$$

with $H_t = \frac{1}{3}$ (for turbulence) measuring the departure from isotropy, and 1_D the identity $D \times D$ matrix (thus isotropic for all purely spatial cuts; note however that atmospheric turbulence has been found [42] to exhibit a scaling anisotropy between the vertical and the two horizontal directions). The operator is characterized by the elliptical dimension D_{el} such that the Jacobian of the transform of Eq. 82 is $\lambda^{-D_{el}}$. Here, this dimension is simply the trace of $\mathcal{G}$, i.e., $D_{el} = D + 1 - H_t$.

The generalized scale function $\|.\|$, introduced in Eqs. 27 and 29 now has the property

$$\|T_\lambda (\underline{x}, t)\| = \lambda^{-1} \|(\underline{x}, t)\| \tag{84}$$

Causality

In the space-time domain, Eq. 41 becomes

$$, \ _\Lambda(\underline{x}, t) = g(\underline{x}, t) \star \gamma_\Lambda (\underline{x}, t) \tag{85}$$

For self-affine, space-time cascades, we are led to consider the filter

$$g(\underline{x}, t) \sim \|(\underline{x}, t)\|^{-\frac{D_{el}}{\alpha}} \tag{86}$$

In order to generate a causal [m] multifractal, the filter g should be defined as a retarded Green's function. Thus g "contains" the main characteristics of the cascade, i.e., anisotropy and causality:

$$g(\underline{x},t) = \begin{cases} \|(\underline{x},t)\|^{-\frac{D_{el}}{\alpha}} & t>0 \\ 0 & t<0 \end{cases} \tag{87}$$

In Fourier space, the determination of an explicit form for g can be quite involved (it is the convolution of $\|(\underline{k},\omega)\|^{-D_{el}/\alpha'}$, $\frac{1}{\alpha}+\frac{1}{\alpha'}=1$, with the Fourier Transform of the Heaviside generalized function). However, one can always choose the simple form [51]

$$\hat{g}(\underline{k},\omega) \sim \frac{1}{|\underline{k}|^{\frac{D_{el}}{\alpha'}} - (i\omega)^{\frac{D_{el}}{\alpha'(1-H_t)}}} \tag{88}$$

The causal generator is therefore the solution of the generalized diffusion equation

$$g^{(-1)}(\underline{x},t) \star {}_{,\Lambda}(\underline{x},t) = \gamma_\Lambda(\underline{x},t) \tag{89}$$

$g^{(-1)}$ corresponding to a fractional space-time differential operator.

For illustration, we can single out two simple examples, both with $\alpha=2$ (the generator has Gaussian statistics): (1) $D=2$ (i.e., two spatial dimensions and one temporal dimension), $H_t=-1$, thus $\tau_\ell \sim \ell^{1/2}$, giving the same anisotropy as for Brownian motion; the diffusion equation reduces to $[\partial_t - \Delta]$, ${}_{,\Lambda}(\underline{x},t) = \gamma_\Lambda(\underline{x},t)$, which is nearly the heat diffusion equation, except for the limited integration domain (γ_Λ is filtered so to remove its components $\|(\underline{k},\omega)\|$ outside of the range $[1;\Lambda]$), responsible for the stationnarity of the generator; (2) $D=1$, $H_t=0$ (isotropic case) giving $[\partial_t + (-\Delta)^{1/2}]$, ${}_{,\Lambda}(x,t) = \gamma_\Lambda(x,t)$; this is to be compared with its purely spatial (i.e., non-causal) version, given for any D by $\hat{g}^{-1}(\underline{k}) = |\underline{k}|^{-1}$. This simple case is indeed at the origin of the model. Note that a non-limited integration domain version of this diffusion equation would lead to an equivalent Langevin description corresponding to "Cauchy flights" [135].

Causal fractionally integrated flux model

For the space-time domain, non-conservative multifractals ρ_Λ, like the turbulent velocity (at least scalar, i.e., corresponding to a single component of

[m] "causal" used here as an abbreviation for "causal antecedence", or even space-time contiguity, as described in [128].

the vector) or the scalar concentration, are deduced from their corresponding fluxes F_Λ through a causal fractional integration of order H:

$$\hat{\rho}_\Lambda(\underline{k},\omega) = \hat{G}(\underline{k},\omega)\ \widehat{F^a_\Lambda}(\underline{k},\omega) \tag{90}$$

with $\hat{G}(\underline{k},\omega)$ being a causal version of $\|(\underline{k},\omega)\|^{-H}$; the simplest choice corresponds to[131]

$$\hat{G}(\underline{k},\omega) \sim \frac{1}{|\underline{k}|^H - (i\omega)^{H/(1-H_t)}} \tag{91}$$

In fact the large flexibility on the choice of the Green's function satisfying the adequate scaling can be used in order to establish some contact with the notions of renormalized viscosity and renormalized forcing. Indeed, Eq. 3 corresponds to:

$$\hat{G}_R^{-1}(\underline{k},\omega)\hat{\underline{u}}(\underline{k},\omega) = \hat{\underline{f}}_R(\underline{k},\omega) \tag{92}$$

where the renormalized Green's function $\hat{G}_R^{-1}$ is of the form:

$$\hat{G}_R^{-1}(\underline{k},\omega) = -i\omega + \nu_R(\underline{k},\omega)k^2 \tag{93}$$

Therefore, Eqs. 92-93 and Eqs. 90-91 are equivalent if:

$$\hat{G}(\underline{k},\omega) \sim \hat{G}_R^{H/(1-H_t)}(\underline{k},\omega) \tag{94}$$

$$\hat{f}_R(\underline{k},\omega) \sim \hat{G}_R^{\frac{H}{1-H_t}-1}(\underline{k},\omega)\widehat{F^a_\Lambda}(\underline{k},\omega) \tag{95}$$

This points out that the renormalized forcing should be rather extremely intermittent, whereas, until now, the analytical/renormalization approaches presupposed a quasi-Gaussian behavior.

We have simulated a causal scalar turbulent velocity shear field on a 2-D (in space) 1-D (in time) domain (Fig. 15), for $\alpha = 1.5$, $H_t = 1/3$, $H = 1/3$, $a = 1$ and $C_1 = 0.1$. Note the longer life-times of the largest structures, compared to the life-times of smaller structures.

4.3 Decorrelation process of causal multifractals

Predictability

The sensitivity of nonlinear dynamics to small perturbations has been widely popularized with the help of the "butterfly effect" metaphore in deterministic chaos (few degrees of freedom). Two flows initially very close in phase-space will tend to diverge exponentially with time, becoming fully uncorrelated in

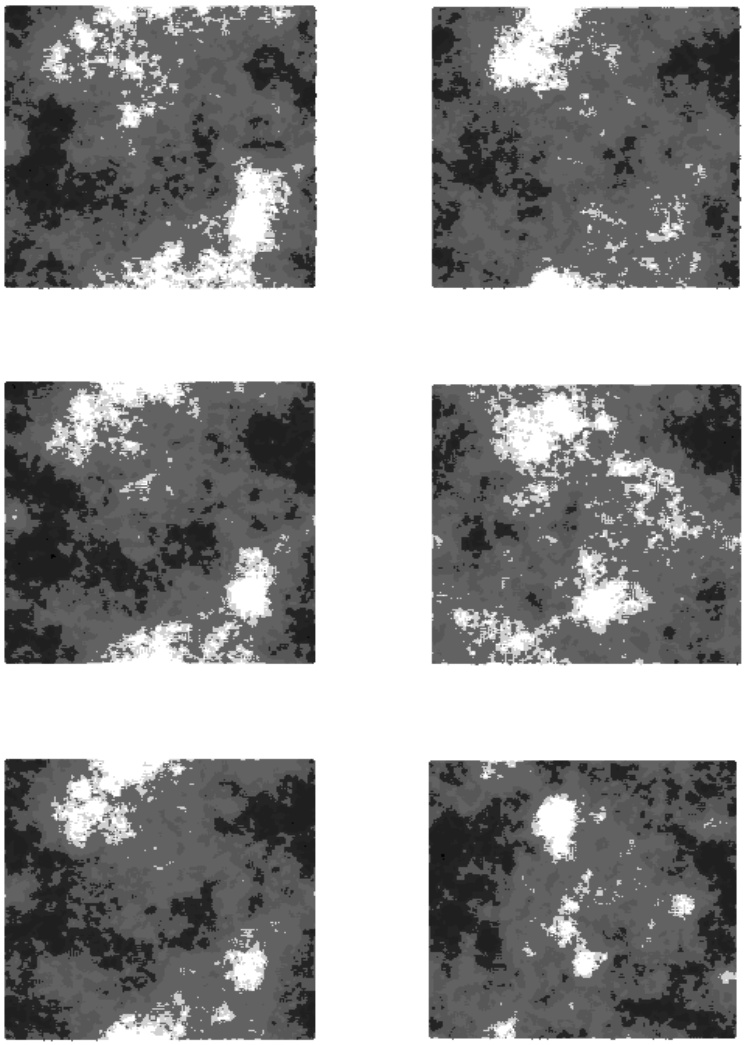

Figure 15: Numerical simulation of a causal turbulent scalar velocity shear field, on a 3-D domain (2-D in space, 1-D in time); $\alpha = 1.5$, $C_1 = 0.1$, $H_t = 1/3$, $H = 1/3$, $a = 1$. We display six spatial 2-D scans, the first scan at the upper left corner, followed by three consecutive scans (at regular intervals corresponding to a time step, the typical life-time of the smallest structures) from center to bottom, left column, and upper right corner, then (from center to bottom, right column) the scans at 8 and 16 time steps after the first scan.

a finite characteristic time (the inverse of which is the Lyapunov exponent). For fully developed turbulence (infinite number of degrees of freedom), due to scaling both in space and time, there is no characteristic time of the process, and one thus expects an algebraic decorrelation in time. The characterization of this phase-space divergence, or decorrelation process, in turbulence has been discussed mainly for atmospheric flows (Lilly[110] and Houtekamer[111] for reviews). Closure techniques for homogeneous turbulence: Quasi-Gaussian approximations[112], the Test-Field model[113], or the EDQNM model[114], lead to a characterization of the temporal evolution of the cross-correlated energy spectrum for two flows initially differing only for wavenumbers larger than an "error cut-off wavenumber" $k_e(t=0)$. These models are intrinsically limited by strong assumptions on the statistics of the solution, thus missing the essential feature of the intermittency of the process. More recently, an approach based on shell-models has been proposed[115,116], defining generalized Lyapunov exponents. However, shell-models drastically lose their spatial dimensionality (see [52] and Sec. 5 for discussion and alternatives) and keep only a very reduced number of degrees of freedom, chosen typically around 30 for numerical purposes; therefore their relevance to turbulence predictability issues remains questionnable.

The causal cascade model for turbulence indeed allows for a complete description of this decorrelation process, i.e. its average behavior given by the classical spectra (second order statistics), as well as its strong variability by considering higher order statistics. It is important to note, as described in Appendix B, that the decorrelation of two fields identical up to a time t_0 and then diverging, as their subgenerators become independent, is statistically similar to the auto-decorrelation in time of a single field. Temporal increments $\Delta\rho_{\Lambda,\Delta t}$ over time-lags Δt:

$$\Delta\rho_{\Lambda,\Delta t}(\underline{x},t) = \rho_\Lambda(\underline{x},t+\Delta t) - \rho_\Lambda(\underline{x},t) \tag{96}$$

are the relevant quantities of interest in order to study this process, not only at all scale, but also at all order (i.e. with help of the corresponding structures functions). A dipole effect (see Appendix A) points out that there should be a sharp contrast between scales larger and smaller than the time lag Δt occuring at all order statistics. Indeed, for scales larger than the time lag, the effective order of fractional integration is decreased, whereas for smaller scales the increments are rather similar to the original field, because the two terms on the r.h.s. of Eq. 96 are independent.

Spectral decorrelation

The engery spectrum of the increments $\Delta\rho_{\Lambda,\Delta t}(\underline{x},t)$ is the spectrum of (auto-) decorrelation:

$$E_{\Delta}(k,\Delta t)\delta(\underline{k}+\underline{k}')|\underline{k}|^{1-D} =< \widehat{\Delta\rho}_{\Lambda,\Delta t}(\underline{k},t)\widehat{\Delta\rho}_{\Lambda,\Delta t}(\underline{k}',t) > \qquad (97)$$

whereas the correlated energy spectrum E_{W_Λ} is:

$$E_{W_\Lambda}(k,\Delta t)\delta(\underline{k}+\underline{k}')|\underline{k}|^{1-D} =< \hat{\rho}_{\Lambda}(\underline{k},t)\hat{\rho}_{\Lambda}(\underline{k}',t+\Delta t) > \qquad (98)$$

and

$$E_{\Lambda}(k) = E_{W_\Lambda}(k,\Delta t) + E_{\Delta_\Lambda}(k,\Delta t),\ \forall\Delta t \qquad (99)$$

where $E_\Lambda(k)$ is the classical spectrum (e.g. giving for $\rho = u$ the Kolmogorov law $k^{-5/3}$) of the field ρ_Λ. The dipole argument yields (Appendix A):

$$k << k_e(\Delta t) \Rightarrow E_{\Delta}(k,\Delta t) \simeq k^{-2}E(k) \qquad (100)$$

$$k >> k_e(\Delta t) \Rightarrow E_{\Delta}(k,\Delta t) \simeq E(k) \qquad (101)$$

and indeed it was shown [131] that:

$$E_{\Delta_\Lambda}(k,\Delta t) = E_\Lambda(k)\ (1-\Phi(k,\Delta t)) \qquad (102)$$

where Φ is a cut-off function of the form $\Phi(k,\Delta t) = \|(1,\frac{k}{k_e(\Delta t)})\|^{-(1+2H)+K(2,a)}$ (the spectral exponent is equal to $-5/3 + K(2,1/3)$ for turbulent velocity), $k_e(\Delta t) \sim \Delta t^{-1/(1-H_t)}$ being the cut-off wavenumber. For $k >> k_e(\Delta t)$, $\phi(k,\Delta t) \sim k^{-(1+2H)+K(2,a)} << 1$ and thus $E_{\Delta_\Lambda}(k,\Delta t) = E_\Lambda(k)$, i.e., the small scales are completely decorrelated, while for $k << k_e(\Delta t)$, $\phi(k,\Delta t) = 1$, and thus $E_{\Delta_\Lambda}(k,\Delta t) = 0$, i.e., the large scales are still completely correlated.

We simulate the decorrelation of a field ρ_Λ with universal parameters $\alpha = 1.1$ and $C_1 = 0.82$, on a 2-D space-time cut (1-D in space and 1-D in time). The anisotropy exponent H_t is taken equal to $H_t = 1/3$, and the field is fractionally integrated (order $H = 1/3$, and $a = 1$). The ensemble average is done on 10000 realizations.

Fig. 16 displays E_{Δ_Λ} for these simulations. Though the large scales ($k << k_e(\Delta t)$) do contain uncorrelated energy, it is clear that it is negligeable compared to the correlated energy at the same scales; with Δt increasing, the cut-off wavenumber $k_e(\Delta t)$ decreases, and the uncorrelated energy spectrum tends to the classical energy spectrum (for our simualtions corresponding to a $k^{-1.75}$ law) over the whole range $k > k_e(\Delta t)$.

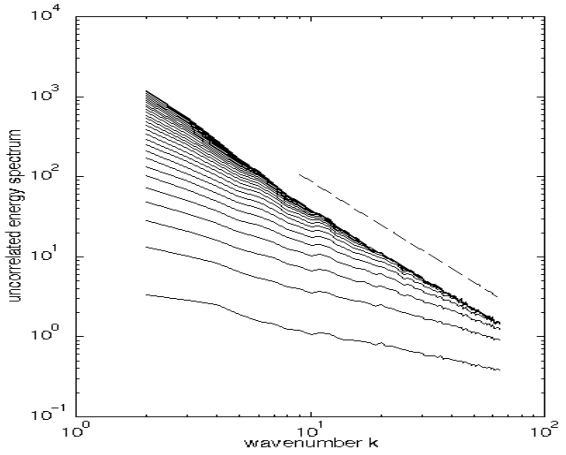

Figure 16: Uncorrelated energy spectra for temporal intervals Δt increasing linearly, from bottom to top. Universal parameters are: $\alpha = 1.1$, $C_1 = 0.82$, and the anistropy was given by $H_t = 1/3$. The field has been fractionally integrated (order $H = 1/3$, $a = 1$). The dashed line corresponds to the $|k|^{-1.75}$ law.

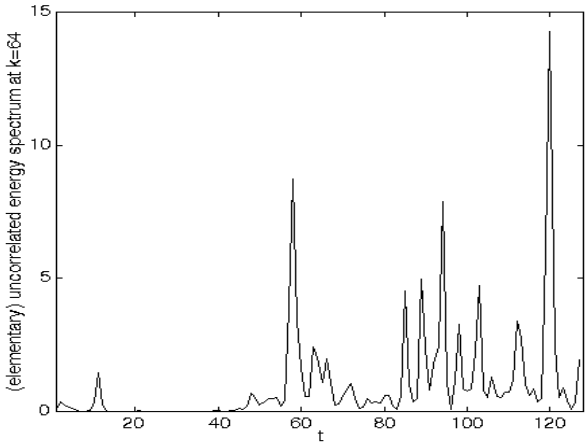

Figure 17: "Elementary" uncorrelated energy spectrum (see text for definition) for Δt equals to the a time-step, i.e. the typical life-time of the structures at smallest scale, for a single realization of the field $\rho\Lambda$, at wavenumber $k = 64$. Same field as in the previous figure.

Quantifying the intermittency of the decorrelation process

However, as already argued in [131], the spectra defined above are not sufficient on their own to account for the intermittency of the decorrelation process. Indeed, Fig. 17 shows, for a single realization of the simulations described for Fig. 16, the quantity $|\widehat{\Delta\rho}_{\Lambda,\Delta t}(k,t)|^2$ for $k = k_{max} = 64$ and $\Delta t = \Delta t_{min} > 0$, thus Δt being the typical life-time of the structures at the smallest scale of resolution. The uncorrelated energy spectrum is the ensemble average of this (stationnary) quantity (called hereafter "elementary" uncorrelated energy spectrum); the process now is seen as being strongly variable, and looks much more like an intermittent succession of violent and sudden "bursts" of decorrelation rather than smooth and predictable. The spectra defined above are only relevant for the prediction of the average behavior of this process.

A crucial question is then how to define the pertinent measures in order to properly quantify the intermittency. As was argued in [131] for fluxes F_Λ, a very straightforward idea would be to define generalized (all order statistics and not only second order statistics) spectra, i.e., correlated and uncorrelated energy spectra of the normalized η-power of F_Λ:

$$E^{(\eta)}_{W_\Lambda}(k,\Delta t)\delta(\underline{k}+\underline{k}')|\underline{k}|^{-1+D} = \frac{< \widehat{F^\eta_\Lambda}(\underline{k},t)\widehat{F^\eta_\Lambda}(\underline{k}',t+\Delta t) >}{< F^\eta_\Lambda >^2} \tag{103}$$

which can be directly deduced from the correlation measure $C^{(1)}_\Lambda(F,\eta,\Delta\underline{x},\Delta t)$ defined in Appendix B (see [131]). It was shown in [131] that, for a given η, such spectra completely characterize the decorrelation process for a single order of singularity $\gamma^{(\eta)}_F$

$$\gamma^{(\eta)}_F = \frac{dK(q=2,\eta)}{dq} \tag{104}$$

thus really corresponding to a mono-fractal measure; among these spectra, we recover for $\eta = 1$ the set of spectra defined in the previous section, which clearly indicates their intrinsic limitation. In the contrary, by letting η vary so that $\gamma^{(\eta)}_F$ explores the whole range of orders of singularity of the multifractal F_Λ, we are able to give a proper account of the complete statistics (average behavior and strong variability) of the process.

For fractionally integrated multifractals ρ_Λ, the equivalent of Eq. 103 is somewhat more involved, and does not seem to be explicitly solvable. However, one can argue that, since the transition from a flux F_Λ to its fractionally integrated form ρ_Λ merely consists in shifting the orders of singularity of F_Λ

by the fractional order H, it is expected that E_{W_Λ} for ρ_Λ indeed singles out the order of singularity $\gamma_\rho^{(\eta)}$ such that

$$\gamma_\rho^{(\eta)} = \frac{dK(q=2,a\eta)}{dq} + H \tag{105}$$

Another approach is to define a different set of measures; indeed, the spectra

$$\mathcal{E}_\Lambda^{(\eta)}(k,\omega)\ \|(\underline{k},\omega)\|^{-D_{el}+1}\delta(\underline{k}+\underline{k}')\delta(\omega+\omega') = \frac{<\widehat{\rho_\Lambda}^\eta(\underline{k},\omega)\widehat{\rho_\Lambda}^\eta(\underline{k}',\omega')>}{<F_\Lambda^{K(a)}>^{2\eta}} \tag{106}$$

are more easily derivable. We derive it for $\eta = 2$ (see Appendix C); an interpolation of this result to all η leads to

$$\mathcal{E}_\Lambda^{(\eta)}(k,\omega) \sim\ \|(k,\omega)\|^{-2H\eta-2(\eta-1)D_{el}-1+K(2\eta,a)} \tag{107}$$

Note that the two known cases ($\eta = 1$ and $\eta = 2$) are retrieved here.

It is easy to check that $\mathcal{E}_\Lambda^{(\eta)}$, in the same way as the generalized spectra $E_{W_\Lambda}^{(\eta)}$ and $E_{\Delta_\Lambda}^{(\eta)}$, singles out for every η a different order of singularity. Therefore, we conclude that the spectra $\mathcal{E}_\Lambda^{(\eta)}$ are indeed pertinent for characterizing the variability of the decorrelation process.

4.4 Forecasting

We now test the forecasting capacity of the causal space-time cascade models. It was already argued in [51] that one can compute a predictor of a flux F_Λ known up to a given time t_0 from the retrieved subgenerator, thus defined up to t_0; indeed, the construction of universal, causal, space-time multifractals can be seen as the causal mapping of the subgenerator $\gamma(\underline{x},t)$ to the multifractal $F_\Lambda(\underline{x},t)$

$$\gamma(\underline{x},t) \longrightarrow F_\Lambda(\underline{x},t) \tag{108}$$

for $(\underline{x},t)$ belonging to a given domain. The inverse operation

$$F_\Lambda(\underline{x},t) \longrightarrow \gamma(\underline{x},t) \tag{109}$$

is naturally possible, and we thus define, for $F_\Lambda(\underline{x},t)$ known up to t_0, the "past" subgenerator $\gamma_p(\underline{x},t)$. A possible realization of the future of F_Λ, thus $F_\Lambda(\underline{x},t=t_0+\Delta t)$, is given by the direct causal mapping of $\gamma(\underline{x},t<t_0+\Delta t)$ such that

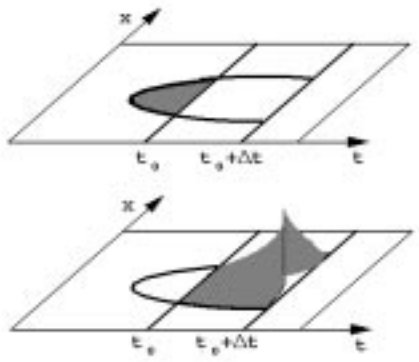

Figure 18: The generation of the two contributions $F_{p,\Lambda}$ and $F_{f,\Lambda}$ to F_Λ. The figure on top shows that $F_{p,\Lambda}$ is constructed by limiting the integration domain of $\gamma_(x,t)$ on the "past" field (in gray), while (bottom figure) the corresponding domain for $F_{p,\Lambda}$ is only on the "future" field, and the generated $F_{f,\Lambda}$ is therefore the result of a space-time cascade with a scale-ratio of $||(1,\Delta t)||$.

$$\gamma(\underline{x},t) = \gamma_p(\underline{x},t),\ t<t_0 \quad (110)$$

$$\gamma(\underline{x},t) = \gamma_f(\underline{x},t),\ t>t_0 \quad (111)$$

where γ_f is a realization of a Lévy white noise (thus independent of γ_p). It is easy to see that $F_\Lambda(\underline{x},t=t_0+\Delta t)$ is decomposable in two multiplicative terms:

$$F_\Lambda(\underline{x},t_0+\Delta t) = F_{p,\Lambda}(\underline{x},t_0+\Delta t)F_{f,\Lambda}(\underline{x},t_0+\Delta t) \quad (112)$$

where the two terms $F_{p,\Lambda}$ and $F_{f,\Lambda}$ have very different meanings: $F_{p,\Lambda}$ is the mapping, in the future, of γ_p; it is thus entirely determined by the past, i.e., from the known values of the field F_Λ up to t_0, and corresponds to a relaxation from the past, known field to 1 (constant in both $\underline{x}$ and t) as Δt increases and eventually reaches 1 (the integral time). In contrast $F_{f,\Lambda}$ is the mapping, in the future, of γ_f; it is thus purely stochastic, does not depend on the past, and corresponds to a normalization term. Thus the optimum forecast of $F_\Lambda(\underline{x},t>t_0)$ given $F_\Lambda(\underline{x},t>t_0)$ is

$$< F^q_\Lambda(\underline{x},t_0+\Delta t)|F_\Lambda(\underline{x},t<t_0) >= F^q_{p,\Lambda}(\underline{x},t_0+\Delta t)\ < F^q_{f,\Lambda}(\underline{x},t_0+\Delta t) > \quad (113)$$

Finally, we note that $< F^q_{f,\Lambda}(\underline{x}, t_0 + \Delta t) > \sim (\Lambda\lambda_\varepsilon^{-1})^{K(q)}$ with $\lambda_\varepsilon^{-1} = \|(1, \Delta t)\|$, since $F_{f,\Lambda}$ simply results from a cascade developed from the cut-off scale λ_ε down to the maximum resolution Λ (see Fig. 18). We then obtain

$$< F^q_\Lambda(\underline{x}, t_0 + \Delta t) | F_\Lambda(\underline{x}, t < t_0) >= F^q_{p,\Lambda}(\underline{x}, t_0 + \Delta t)\ (\Lambda\lambda_\varepsilon^{-1})^{K(q)} \qquad (114)$$

A similar development can be obtained for the fractionally integrated field ρ_Λ; however, an explicit expression corresponding to Eq. 114, in this case of a non-conservative multifractal, does not seem to be easily derivable. An exception is for the moment of order 1, giving

$$< \rho_\Lambda(\underline{x}, t_0 + \Delta t) | \rho_\Lambda(\underline{x}, t < t_0) >= \rho_{p,\Lambda}(\underline{x}, t_0 + \Delta t) \qquad (115)$$

where $\rho_{p,\Lambda}(\underline{x}, t) = G(\underline{x}, t) \star F^a_{p,\Lambda}(\underline{x}, t)$. An exemple is given in Fig. 19; we display the predicted field $< \rho_\Lambda(x, t_0 + \Delta t) | \rho_\Lambda(x, t < t_0) >$ for a simulated $\rho_\Lambda(x, t < t_0)$ (see caption for parameters). Since, for the moment of order 1, the normalization term is equal to 1, as given by Eq. 115, we observe here only the relaxation term. The predicted signal is then merely a filtered signal, since at Δt, all the components at wavenumbers k such that $k > k_e(\Delta t)$ are smoothed out.

5 Scaling Gyroscopes Cascade (SGC)

5.1 Shell-models and beyond...

The complexity and unsolvability of the Navier-Stokes equations have lead to the consideration of some simplified caricatures of them, which nevertheless preserve some fundamental properties of the original ones. One well-known example is the Burgers equation, which as a 1-D turbulence model gives precious hints on intermittency although it has unfortunately the drawback of introducing compressibility. The so-called "shell-models" [57,58] have been very popular caricatures of Navier-Stokes equations from which they conserve the quadratic interaction and invariance for the flux of energy, however in an extremely simplified framework since they are only scalar (not vector) models and retain only the spatial scale dependence instead of location dependence. Indeed, these models consider the time evolution of the averaged characteristic velocity shear u_n (with corresponding vorticity $k_n u_n$) on the shell defined by the wave-vectors $|\underline{k}| \simeq k_n$, the wave-number k_n being the inverse of scale of the corresponding eddies which is discretized in a exponential way ($l_n = L/\lambda^n$, L being the outer scale). Their equation of evolution is of the following type:

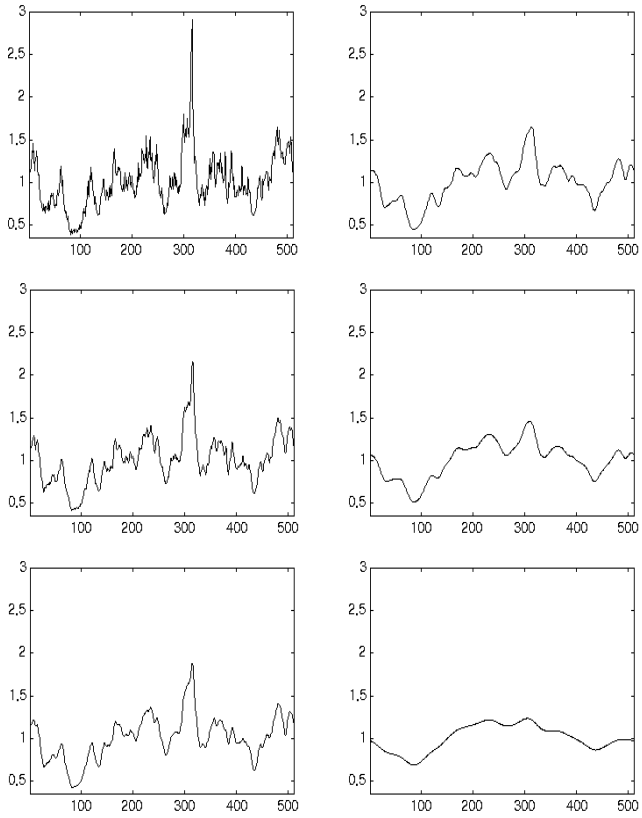

Figure 19: An exemple of predicted $\rho_\Lambda(x, t = \Delta t + t_0)$, for a 2-D cut (1-D in space and 1-D in time); parameters are: $\alpha = 1.5$, $C_1 = 0.15$, $H_t = 1/3$, $H = 1/3$, $a = 1$, $\Lambda = 512$. We display 1-D spatial cuts of the field at $\Delta t = 1, 2, 3, 5, 9$ and 20 times the typical life-time at the smallest scale (from top to bottom and left to right).

$$\left(\frac{d}{dt}+\nu k_n^2\right) u_n = k_n u_n u_{n-1} - k_{n+1} u_{n+1}^2 \tag{116}$$

We will show below that these models correspond to an over simplification of a more complete model. This model, which is obtained by keeping only certain type of interactions of the Navier-Stokes equations, is indeed needed since the spatial dimension is absent in shell-models, whereas it is crucial for the development of intermittency. The relevance of this drastic dimensional reduction was already questioned [52,118], as well as the relevance of models having a number of eddies which do not increase algebraically with the inverse of the scale. Indeed this number $N(\ell)$ should scale as $N(\ell) \sim \ell^{-D}$, where ℓ is the scale and D is the dimension of the model. D can be lower than the dimension of the turbulence itself (e.g. for a D-dimensional cut, D being a number independent of the scale [119]).

In order to take into account the spatial dimension, while keeping an exponential discretization of scales (which is not manageable with fast Fourier transforms), we introduce a tree structure of eddies: each eddy having $N(\lambda) = \lambda^D$ sub-eddies whose location is labeled by (i) (in correspondence to its center $\underline{x}_n^i$, the distance between two neighboring centers being of the order of l_n). This type of space and scale analysis has been widely used for phenomenological cascade models and is indeed a precursor of orthogonal wavelet decompositions [120]. To the eddy of size l_n and a location $\underline{x}_n^i$ corresponds a velocity field $(\underline{\widehat{u}}_n^i)$ and vorticity field $(\underline{\widehat{w}}_n^i)$ Fourier/wavelet components, as well as the corresponding wave-vector $(\underline{k}_n^i)$:

$$\underline{\widehat{u}}_n^i \equiv \underline{\widehat{u}}(\underline{k}_n^i) \; ; \quad \underline{\widehat{w}}_n^i = i\underline{k}_n^i \wedge \underline{\widehat{u}}_n^i \; ; \quad k_n = |\underline{k}_n^i| \tag{117}$$

Along this tree-structure, we show that for 3-D turbulence as well as for 2-D turbulence, the equations of evolution due to direct interactions between eddies and sub-eddies are analogous to the Euler equations of a gyroscope. The corresponding indirect interactions are obtained by coupling an infinite hierarchy of gyroscopes. Overall we derive from rather abstract considerations on the structure of the Navier-Stokes equations (its Lie structure) dynamical space-time models which can be called Scaling Gyroscope Cascade (SGC) models. It is interesting to note that the recognition of the similarities [54,55] between the Navier-Stokes equations of hydrodynamic turbulence and the Euler equations of a gyroscope can be traced back to Lamb [53].

The SGC yields concrete models which can be used to investigate fundamental questions of turbulence, in particular its intermittency. Not only does the SGC yield the inverse energy cascade sub-range as well as the direct enstrophy sub-range for the two-dimensional turbulence, but the multifractal

characteristics of the former are extremely close to those of the direct energy cascade of three-dimensional turbulence. We also find a surprisingly close agreement with various empirical studies of atmospheric turbulence.

5.2 Navier-Stokes equations and Euler equations of a gyroscope; Arnold's analogy

Consider the Navier-Stokes equations, for the velocity field $\underline{u}(\underline{x},t)$, written in the Bernoulli form (α being the kinematic pressure, i.e. for barotropic flows: $\alpha = \int \frac{dp}{\rho(p)} + \frac{u^2}{2}$, p being the (static) pressure; ν is the fluid viscosity):

$$\left(\frac{\partial}{\partial t} - \nu\Delta\right)\underline{u}(\underline{x},t) = \underline{L}(\underline{x},t) - \underline{grad}(\alpha) \tag{118}$$

where $\underline{L}$ is the Lamb vector and $\underline{w}$ is the vorticity field:

$$\underline{L}(\underline{x},t) = \underline{u}(\underline{x},t) \wedge \underline{w}(\underline{x},t) \tag{119}$$

$$\underline{w}(\underline{x},t) = \underline{curl}(\underline{u}(\underline{x},t)) \tag{120}$$

with the associated incompressibility condition:

$$div(\underline{u}(\underline{x},t)) = 0 \ . \tag{121}$$

The curl of Bernoulli's equation (Eq. 118) corresponds to the well known vorticity equation:

$$\left(\frac{\partial}{\partial t} - \nu\Delta\right)\underline{w}(\underline{x},t) = [\underline{w}(\underline{x},t), \underline{u}(\underline{x},t)] \tag{122}$$

the Lie bracket then being defined as:

$$[X,Y] = \underline{Y} \cdot \underline{\underline{grad}}(\underline{X}) - \underline{X} \cdot \underline{\underline{grad}}(\underline{Y}) \tag{123}$$

The analogy pointed out by Arnold [54] is between the vorticity equation (Eq. 122) and Euler's gyroscope equation.

Consider the first Euler's theorem or Euler's gyroscope equation (i.e., equation for a rotating rigid body attached to a fixed point with no torque):

$$\frac{d\underline{M}}{dt} = [\underline{M}, \underline{\Omega}] \equiv \underline{M} \wedge \underline{\Omega} \tag{124}$$

where $\underline{M}$ is its angular momentum and $\underline{\Omega}$ its rotation (both relative to the body frame); the Lie bracket being defined by the vector product $\wedge$. The

(quadratic) non linearity of this (apparently linear) equation results from the linear relationship between angular momentum and rotation via the (second order) moment of inertia tensor $\underline{\underline{I}}$ or its inverse ($\underline{\underline{J}} = \underline{\underline{I}}^{-1}$), both being symmetric:

$$\underline{M} = \underline{\underline{I}} \cdot \underline{\Omega} \; ; \quad \underline{\Omega} = \underline{\underline{J}} \cdot \underline{M} \tag{125}$$

Therefore, the gyroscope equation is quadratic in the angular momentum. The equation of motion relative to the body frame (Eq. 124) is equivalent to Newton's law of the conservation of angular momentum relative to space (M_s):

$$\frac{dM_s}{dt} = 0 \tag{126}$$

This second Euler's theorem is in fact a particular case of Noether's theorem stating that there is an invariant associated with every equation of motion. There are two associated quadratic invariants to (Eq. 124), the first one being the square of the angular momentum (M^2). The second quadratic invariant is the kinetic energy of the body:

$$T = \frac{1}{2} \, \underline{M} \cdot \underline{\Omega} \equiv \frac{1}{2} \, \underline{M} \cdot (\underline{\underline{J}} \cdot \underline{M}) \tag{127}$$

One may note that the Fourier components of the fields require us to consider the rather straightforward extension to complex gyroscopes (complex conjugates being denoted by an overbar):

$$\frac{d\overline{\underline{M}}}{dt} = [\underline{M}, \underline{\Omega}] \tag{128}$$

The Hermitian extension of the Euclidean structure preserves the quadratic invariants, since the notion of mixed product (denoted by $(.,.,.))$ [n] is unchanged:

$$\frac{dT}{dt} = \Re(\underline{M}, \underline{\Omega}, \underline{\Omega}) \equiv 0 \; ; \qquad \frac{dM^2}{dt} = 2\Re(\underline{M}, \underline{\Omega}, \underline{M}) \equiv 0 \tag{129}$$

$\Re$ denoting the real part of complex variable.

In the perspective of Arnold's analogy, the vorticity and the velocity are respectively the analogues of the angular momentum ($\underline{M}$) and of the rotation ($\underline{\Omega}$), the field analogue of the inertial tensor, is the *curl*. However, there are fundamental differences between their respective Lie algebra. Indeed, while the Lie algebra ($so(3)$) corresponding to Euler's gyroscope, associated with the Lie

[n] $(\underline{a}, \underline{b}, \underline{c}) = \underline{a} \cdot (\underline{b} \wedge \underline{c})$.

group ($SO(3)$) of rotations in the three-dimensional space, is finite (since it can be defined as the set of three dimensional vectors ($\Re^3$) with the vector product (Eq. 124)), the Lie algebra corresponding to the vorticity equation (on a subset D of $\Re^3$) is infinite. Indeed, the latter can be defined as being the set of divergence-free vector fields and it is associated with the group (being noted SDiff D by Arnold) of the one-to-one volume preserving transformations of D. Both are obviously infinite[o]. The infinite dimensionality is not only related to the intervention of partial instead of ordinary differentiations, as well as to the field nature of the velocity, but fundamentally to the phenomenology of fully developed turbulence. Indeed, an infinite number of degrees of freedom should intervene when considering the singular limit of the viscosity going to zero (or correspondingly the Reynolds number going to infinity): one expects the development of a spectrum similar to the Kolmogorov-Obukhov spectrum [3,4] down to a viscous scale which goes to zero, i.e. a range of scales[p] goes to infinity. A linear drag can be introduced into Euler's gyroscope equation (Eq. 124) in analogy to the viscous term of Navier-Stokes equation (Eq. 118). However, the singular perturbation corresponding to the latter has a global effect by creating a flow of energy down to smaller scales in 3-D turbulence (of enstrophy in 2-D turbulence), although it intervenes *directly* only in the viscous range. This fundamental scale problem clearly points out the necessity of dealing with an infinite dimensional Lie algebra. As shown in the following sections, it rather involves an infinite hierarchy of gyroscopes rather than being analogous to one of them. Furthermore, even for a finite number of modes, the Lie bracket (Eq. 123) defined by the vorticity equation (Eq. 120) does not correspond to the vector product. It is not dimensionless and introduces therefore a scale dependency. However, it is relevant for 2-D turbulence, but in a new context.

5.3 Analogy based on the Lie structure of turbulence

For 3-D turbulence an analogy rather opposite to Arnold's one can be considered: the velocity, the vorticity, the energy and the helicity are respectively the analogues of the angular momentum ($\underline{M}$), of the angular velocity ($\underline{\Omega}$), of the square of the momentum (M^2) and of the energy ($\underline{M} \cdot \underline{\Omega}$). This analogy can be better appreciated when one considers interactions which yield a divergence-less Lamb vector. Indeed, the pressure gradient does not intervene any longer (since it is only needed to enforce incompressibility) in the r.h.s. of

[o] It might be important to note that the intrinsic dimensions of the algebra or groups, are not to be confused with the dimension of the spaces on which one of their representations acts. Indeed, the latter could be infinite even in the case of a finite algebra.

[p] However, as discussed in the next section, the number of degrees of freedom is larger than the range of scales.

Bernoulli's equation (Eqs. 118-120) which is therefore analogous to the Euler equation (Eq. 124):

$$\left(\frac{\partial}{\partial t} - \nu\Delta\right) \underline{u}(\underline{x},t) = \underline{u}(\underline{x},t) \wedge \underline{w}(\underline{x},t) \tag{130}$$

More generally, one may introduce in the Bernoulli equation (Eq. 118) instead of the pressure gradient the projector $\underline{\underline{P}}(\underline{\nabla})$ (resp. $\underline{\underline{\widehat{P}}}(\underline{k})$ in Fourier space) on divergence-free vector fields :

$$P_{i,j}(\underline{\nabla}) = \delta_{i,j} - \nabla_i \nabla_j \Delta^{-1} \; ; \qquad \widehat{P}_{i,j}(\underline{k}) = \delta_{i,j} - k_i k_j / k^2 \tag{131}$$

which yields[q] an expression (either in physical space or in Fourier space) rather similar to the Euler equations of rigid body motion (Eq. 124):

$$\left(\frac{\partial}{\partial t} - \nu\Delta\right) \underline{u}(\underline{x},t) = \underline{\underline{P}}(\underline{\nabla}) \cdot \underline{u}(\underline{x},t) \wedge \underline{w}(\underline{x},t) \tag{132}$$

$$\left(\frac{\partial}{\partial t} + \nu k^2\right) \underline{\widehat{u}}(\underline{k},t) = \underline{\underline{\widehat{P}}}(\underline{k}) \cdot \int_{\underline{k}+\underline{p}+\underline{q}=\underline{0}} \underline{\widehat{u}}(\underline{p},t) \wedge \underline{\widehat{w}}(\underline{q},t) d\underline{p} \tag{133}$$

In a general manner, the Navier-Stokes equations (in the Fourier space) for 3-D turbulence corresponds to an infinite hierarchy of gyroscope-type equations. The (complex) analogues of $\underline{M}$ and $\underline{\Omega}$ being respectively the triplet $(\underline{u}(\underline{k}), \underline{u}(\underline{p}), \underline{u}(\underline{q}))$ and $(\underline{w}(\underline{k}), \underline{w}(\underline{p}), \underline{w}(\underline{q}))$ of a triad $(\underline{k} + \underline{p} + \underline{q} = \underline{0})$ of direct interactions, the Lie bracket being the vector product modulated by the projector $\underline{\underline{\widehat{P}}}(\underline{k})$.

It is well known that 2-D turbulence is rather peculiar, since it has a family of invariants rather different from the 3-D case (or from any extensions to dimensions $d > 2$). This is due to the simple fact that the vorticity ($\underline{\omega}$), as well as the potential vector ($\underline{\Psi}$) of a 2-D flow are orthogonal to the plane of the flow and are therefore defined by their scalar components along the axis perpendicular to the flow:

$$\underline{\omega} = \omega \underline{z} \; ; \qquad \underline{\Psi} = \Psi \underline{z} \; ; \qquad \omega = -\Delta\Psi \tag{134}$$

Ψ being the stream function, $\underline{z}$ is the unit vector in the z direction. This orthogonality introduces some simplifications in the vorticity equation (Eq. 122) and its corresponding Lie bracket (Eq. 123):

$$[\underline{w}(\underline{x},t), \underline{u}(\underline{x},t)] = -\underline{u}(\underline{x},t) \cdot \underline{\underline{grad}}(\underline{w}(\underline{x},t)) \tag{135}$$

[q] Indeed $\underline{\underline{P}}(\underline{\nabla})(\underline{u}) = \underline{u}$ and $\underline{\underline{P}}(\underline{\nabla})(\underline{\underline{grad}}(\alpha)) = \underline{0}$.

there is only advection, the stretching term ($\underline{w} \cdot \underline{\underline{grad}}(\underline{u})$) being strictly zero. This introduces the enstrophy (ω^2) as a second quadratic invariant, whereas the helicity ($\underline{\omega} \cdot \underline{u}$) is strictly zero. The Fourier transform of the vorticity equation:

$$\left(\frac{\partial}{\partial t} + \nu k^2\right) \overline{\widehat{\omega}}(\underline{k},t) = \int_{\underline{k}+\underline{p}+\underline{q}=\underline{0}} d^2\underline{p} \ \left[\Psi(\underline{p}), \omega(\underline{q})\right] \tag{136}$$

involves the following Lie bracket:

$$\left[\Psi(\underline{p}), \omega(\underline{q})\right] = \frac{1}{2}(\underline{q},\underline{p},\underline{z}) \left(\widehat{\Psi}(\underline{p})\widehat{\omega}(\underline{q}) - \widehat{\omega}(\underline{p})\widehat{\Psi}(\underline{q})\right) \tag{137}$$

and corresponds to an infinite hierarchy of gyroscope-type equations. The (complex) analogues of $\underline{M}$ and $\underline{\Omega}$ being respectively the vectors ($\omega(\underline{k})$, $\omega(\underline{p})$, $\omega(\underline{q})$) and ($\Psi(\underline{k})$, $\Psi(\underline{p})$, $\Psi(\underline{q})$) of a triad ($\underline{k}+\underline{p}+\underline{q} = \underline{0}$) of direct interactions. The enstrophy is therefore the analogue of the square of the momentum, whereas the (turbulent) energy is the analogue of the energy of the gyroscope. The Laplacian is the analogue of the inverse of the inertial tensor.

5.4 Discretization of Scaling Cascades of Gyroscopes

The projector $\underline{\underline{\widehat{P}}}(\underline{k})$ (Eq. 133) corresponds to the velocity-vorticity vertex of interactions for a triad of wave vectors ($\underline{k}$, $\underline{p}$, $\underline{q}$) maintaining merely the orthogonality condition corresponding to incompressibility (Eq. 121):

$$\underline{k} \cdot \widehat{\underline{u}}(\underline{k},t) = 0 \tag{138}$$

it has the advantage of being dimensionless.

However, this projector reduces[52] at first order to the identity for nonlocal direct [8] interactions ($max(\underline{k},\underline{p},\underline{q}) \geq \lambda min(\underline{k},\underline{p},\underline{q})$, λ being the arbitrary nonlocalness parameter) which satisfy some orthogonal conditions ($\{|\underline{k}| \ll |\underline{p}| \simeq |\underline{q}|$ and $\underline{p} \perp \underline{k}\}$ and $\{|\underline{p}| \ll |\underline{k}| \simeq |\underline{q}|$ and $\widehat{\underline{u}}(\underline{p}) \| \underline{k}\}$). This nonlocal orthogonal approximation yields estimates of the renormalized forcing and viscosity (see Sect. 1.2) of Eq. 133:

$$\left(\frac{\partial}{\partial t} + \nu k^2\right) \overline{\widehat{\underline{u}}}(\underline{k}) = \int_{|\underline{p}| \geq \lambda |\underline{k}|} \widehat{\underline{u}}(\underline{p}) \wedge \overline{\widehat{\underline{w}}}(\underline{p}) d^d\underline{p} + \left(\int_{|\underline{p}| \leq \lambda^{-1}|\underline{k}|} \widehat{\underline{u}}(\underline{p}) d^d\underline{p}\right) \wedge \overline{\widehat{\underline{w}}}(\underline{k}) \tag{139}$$

The similarity considered in Sect. 5.3 is more obvious after discretization of nonlocal orthogonal approximation along the tree-structure of interactions (see Fig. 5.4) based on the fundamental triads of (direct) interactions ($\underline{k}^i_{n-1}$, $\underline{k}^{2i-1}_n$, $\underline{k}^{2i}_n$), between a mother and two daughter eddies ($i = \overline{1, 2^{n-1}}$). And for

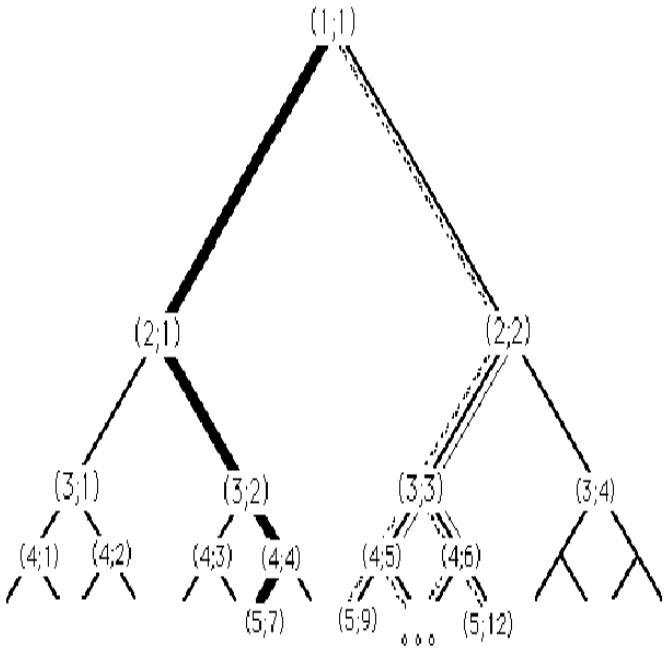

Figure 20: Schematic diagramme of a discrete Scaling Gyroscope Cascade model. In this one dimensional cut, each eddy is a daughter of a larger scale eddy and the mother of two smaller scale eddies. The light thin line indicates interactions for eddy (3;3) in 3-D turbulence, whereas the dashed line indicates its interactions in 2-D turbulence. The thick line points out one of the possible most energetic paths, corresponding to a possible reduction to a shell-model.

3-D turbulence, one obtains [52] the following equation of evolution (omitting temporarily the interactions outside of the triad $(\underline{k}^i_{n-1}, \underline{k}^{2i-1}_n, \underline{k}^{2i}_n)$ as well as the viscous term) for the analogues of the momentum $(\underline{\widehat{M}})$ and of angular velocity $(\underline{\widehat{\Omega}})$:

$$\frac{d\overline{\underline{\widehat{M}}}^i_{n-1}}{dt} = \underline{\widehat{M}}^i_{n-1} \wedge \underline{\widehat{\Omega}}^i_{n-1} \; ; \qquad \overline{\underline{\widehat{\Omega}}}^i_{n-1} = \underline{\underline{J}}^i_{n-1} \cdot \underline{\widehat{M}}^i_{n-1} \tag{140}$$

with the following matrix representations:

$$\begin{bmatrix} \widehat{u}^{2i}_n \\ \widehat{u}^i_{n-1} \\ \widehat{u}^{2i-1}_n \end{bmatrix} = \left[\widehat{M}^i_{n-1}\right] \; ; \qquad \begin{bmatrix} \widehat{\omega}^{2i-1}_n \\ 0 \\ \widehat{\omega}^{2i}_n \end{bmatrix} = \left[\widehat{\Omega}^i_{n-1}\right] \tag{141}$$

and the analogue $(\underline{\underline{J}}^i_{n-1})$ of the projection of inverse of the inertia tensor on the triad corresponds to:

$$\underline{\underline{J}}^i_{n-1} = k_n \underline{\underline{K}} \; ; \qquad [K] = \begin{bmatrix} 0 & 0 & 1 \\ 0 & 0 & 0 \\ 1 & 0 & 0 \end{bmatrix} \tag{142}$$

The equation of evolution of $\underline{\widehat{u}}^j_m$ corresponds therefore to the coupling of two equations of gyroscope type (Eq. 140), therefore to the following (in general complex) scalar equation of evolution for the velocity amplitude $\widehat{u}^j_m$ of the wave vector $\underline{k}^j_m$:

$$\left(\frac{d}{dt} + \nu k_m^2\right) \overline{\widehat{u}}^j_m = k_{m+1} \left[|\widehat{u}^{2j-1}_{m+1}|^2 - |\widehat{u}^{2j}_{m+1}|^2\right] + (-1)^j k_m \overline{\widehat{u}}^j_m \widehat{u}^{a(j)}_{m-1} \tag{143}$$

$a(j)$ being the location index of its "ancestor" $(= E\left(\frac{j+1}{2}\right))$, $E(x)$ being the integer part of the real x $(E(x) \leq x < E(x)+1$). On this equation, the two first terms of the r.h.s. correspond to a renormalized forcing, whereas the last one to the renormalized viscosity.

The SGC model for 3-D turbulence can be reduced to the shell-model defined by Eq. 116, as soon as one observes (as done on a similar model [56]) that at each time there is a most active path on the tree connecting the largest structures to the smallest ones (with a unique eddy at each level) along which most of the energy transfer occurs (see Fig. 5.4). This very crude understanding

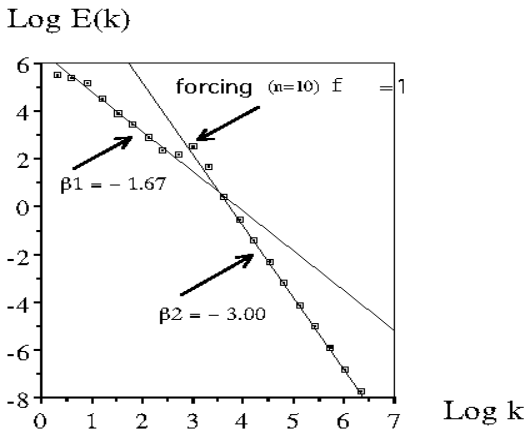

Figure 21: The energy spectrum (averaged over 1024 realizations) of the SGC for 2-D turbulence (forcing at level $n = 10$) displays an inverse energy cascade for low wave numbers (levels $n < 10$) with an algebraic slope close to $\beta_1 = 1.67$, as well as a direct cascade of enstrophy for high wave numbers (levels $n > 10$), with a slope close to $\beta_2 = 3.0$. Logs are base 10.

of intermittency corresponds to eliminating the spatial index j in Eq. 143 with the very unfortunate consequence of eliminating the crucial spatial dimension, as discussed above.

The first order approximation used for discretization in the case of 3-D turbulence cancels in the 2-D case since the Lie bracket (Eq. 137) is strictly zero for any interaction triad having two parallel wave-vectors. One has therefore to consider a second order approximation [118]: instead of considering direct interactions between eddies of two successive levels (mother and daughters), one has to consider interactions between three successive levels (mother, daughter and grand-daughter). This implies (see Fig. 5.4) that direct interactions link a given level (m) of the cascade to the two previous ones ($m-1$, $m-2$) as well as to the two following ones ($m+1$, $m+2$). This yields an algebra more involved than for the case of 3-D turbulence (Eq. 143) and which is generated

by commutators of $\widehat{\Psi}$ and $\widehat{\omega}$:

$$C^{i,i'}_{n,n'} = (\underline{q}^{i'}_{n'}, \underline{p}^{i}_{n}, \underline{z})[\Psi(\underline{p}^{i}_{n}), \omega(\underline{q}^{i'}_{n'})]$$

$$\left(\frac{\partial}{\partial t} + \nu k^2_m\right)\widehat{\omega}^j_m = C^{a(j),a(a(j))}_{m-1,m-2} + \sum_{d(j)=2^{2j-1},2^{2j}}(C^{d(j),a(j)}_{m+1,m-1} + \sum_{d^2(j)=2^{4j-2},2^{4j}} C^{d^2(j),d(j)}_{m+2,m}) \tag{144}$$

The analogues of the energy and of the square of angular momentum are indeed invariant, since we have the detailed conservation laws (similar to Eq. 129) for any triad $((\underline{k},\underline{p},\underline{q}); \underline{k}+\underline{p}+\underline{q}=\underline{0})$:

$$[\Psi(\underline{p}),\omega(\underline{q})]\Psi(\underline{k}) + [\Psi(\underline{q}),\omega(\underline{k})]\Psi(\underline{p}) + [\Psi(\underline{k}),\omega(\underline{p})]\Psi(\underline{q}) = 0 \tag{145}$$

$$[\Psi(\underline{p}),\omega(\underline{q})]\omega(\underline{k}) + [\Psi(\underline{q}),\omega(\underline{k})]\omega(\underline{p}) + [\Psi(\underline{k}),\omega(\underline{p})]\omega(\underline{q}) = 0 \tag{146}$$

Due to the existence of these two invariants, the SGC yields a spectrum subrange (with slope $-\frac{5}{3}$) which corresponds to an inverse energy cascade as well as spectrum subrange (with slope -3) which corresponds to a direct enstrophy cascade (see Fig. 5.4).

5.5 Multifractal features of SGC

Contrary to the multiplicative processes [17,125] the SGC models are fundamentally deterministic: only the forcing could be stochastic. However, it was checked that the SGC is rather independent [52] of the type of forcing used. Therefore, we used for simulations a constant unit forcing which intervenes only at a given level of the cascade (on the level $n = 1$ and on the level $n = 10$ for the 3-D case and the 2-D case respectively). Long runs for large Reynolds numbers (e.g. 1024 large eddy turn-over times) are easily performed on work stations, using inaccurate fourth-order Runge-Kutta scheme. In order to exhibit clearly the two scaling subranges for 2-D turbulence simulations were used 32 levels of the SGC and for 3-D turbulence simulations 19 levels of the SGC yielding $Re \simeq 6 \cdot 10^7$. Spectra in the 3-D case simulations display [52] an absolute slope close to the Kolmogorov-Obukhov [34] $\beta = \frac{5}{3}$ which corresponds to the trivial scaling of Eq. 143 when assuming a constant flux of energy. Spectra of 2-D case simulations (Fig. 5.4) yield clearly the energy subrange (algebraic slope extremely close to $\beta_1 = 1.67$) as well as the enstrophy subrange (slope extremely close to $\beta_2 = 3.0$).

However, spectra do not give direct insights on intermittency. We characterized this intermittency in the framework of universal multifractals. 3-D SGC

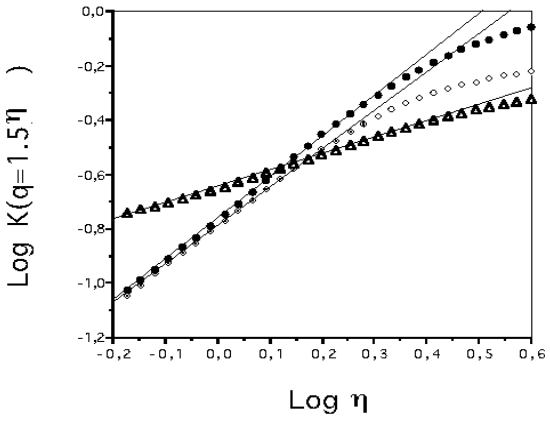

Figure 22: Curves of DTM with the order of moment $q = 1.5$ for 3-D SGC at medium level $n = 7$ and its corresponding "shell-model": $\circ$ - the spatial flux of energy of SGC ($\alpha = 1.4 \pm 0.05$ (the slope of the curves) and $C_1 = 0.25 \pm 0.05$ (the intercept with the vertical axis)); $\bullet$ - the time series of energy flux of SGC ($\alpha = 1.5 \pm 0.05$, $C_1 = 0.25 \pm 0.05$); $\triangleleft$ - the time series of energy flux of "shell-model" ($\alpha = 0.6 \pm 0.05$, $C_1 = 0.4 \pm 0.05$). The latter estimate with $\alpha < 1$ qualitative different behavior of multifractality: singularities are bounded.

numerical simulations clearly support (Fig. 5.5) strong universality (Sect. 2.2) (the misnamed Log-Lévy processes) rather than weak universality (e.g. log-Poisson statistics), only the former possess attractive and stable properties. Log-Lévy statistics of (conservative) fluxes are defined by only two parameters: the mean fractality C_1 and the Lévy index α of multifractality. We estimate (Fig. 5.4) them by a DTM analysis (Sect. 2.4) with an order of moment $q = 1.5$, starting from the level 7 of 3-D SGC simulations. Similar results were obtained with various values of order of moments $q \in (0.8, 2)$. These results, $C_1 = 0.25 \pm 0.05$, $\alpha = 1.4 \pm 0.05$ for the spatial flux of energy of SGC and $C_1 = 0.25 \pm 0.05$, $\alpha = 1.5 \pm 0.05$ for the time series of energy flux of SGC are close to those obtained for atmospheric turbulence [25,117,83,109]. On the contrary, the one-path model or shell model (Eq. 116) for 3-D turbulence yields $C_1 = 0.4 \pm 0.05$ and $\alpha = 0.6 \pm 0.05$. The latter estimate with $\alpha < 1$ corresponds to qualitative different behavior of multifractality[37,68]: singularities are bounded, whereas they are unbounded for $\alpha \geq 1$.

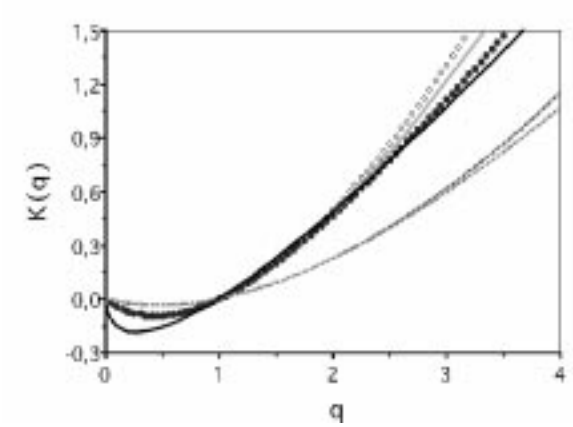

Figure 23: Estimate of the scaling function $K(q)$ obtained on the SGC runs (dotted line), as well as the theoretical curves corresponding respectively to the strong universal multifractal corresponding to the SGC ($C_1 = 0.25,\ \alpha = 1.5$), to the weak universal multifractal (dashed lines) based on the She and Leveque choice of parameters, and its approximation by a corresponding strong universal multifractal (i.e. $C_1 = 0.11$ and $\alpha = 1.62$). Solid lines correspond to empirical and theoretical curves $K(q)$ obtained for "shell-model" with $\alpha = 0.6 \pm 0.05$ and $C_1 = 0.4 \pm 0.05$.

Conclusions

We have argued that intermittency is a fundamental aspect of fully developed turbulence and can only be understood as the result of cascade processes acting over wide ranges of scales involving a large number of degrees of freedom. We first reviewed some of the salient features of cascades emphasizing their generic multifractal limit and some basic multifractal properties (including multifractal phase transitions and the link with self-organized criticality). We argued that - just as for low-dimensional chaos - that without the existence of stable, attractive universality classes, that multifractals would involve an infinite number of parameters and would hence be unmanageable. They would be useless both theoretically and empirically. Fortunately, both strong and weak types of universality classes exist; we outlined the current state of the debate and showed - using turbulent velocity and temperature data - that only strong universality is compatible with the data for both weak and extreme events. Since it has not yet been convincingly demonstrated that the weak universality classes are really attractive, this may not be too surprising; in any case it clearly poses the question as to which is the physically appropriate route to universality ("nonlinear mixing", "scale densification", a combination

of the two, or other).

The bulk of the paper was devoted to developing cascades in two directions. First, we show how they can be used for anisotropic, causal, continuous, space-time turbulence modelling. This takes us far beyond the usual static, discrete, isotropic and acausal multifractal processes which dominate the multifractal literature. On the other hand, we address the fundamental criticism of multifractal turbulence modelling: the gap between the phenomenological (and stochastic) cascades and the dynamical (and deterministic) equations. The history of the attempts to overcome this gap go back over twenty five years to the development of shell models. Collectively, these are systematic sets of approximations to the Navier-Stokes equations which keep many of the symmetries (such as quadratic invariants) and scaling but reduce the nonlinear interactions to a fixed finite (and small) number per wavenumber octave. We show that a more consistent set of approximations (in 2-D as well as in 3-D turbulence) maintains the spatial dimensionality and a number of degrees of freedom increasing algebraically with wavenumber, and yields a Scaling Gyroscopes Cascade model. We show numerically that (contrary to shell models), that this is in nearly an identical universality class to the turbulence data.

These developments furthermore point out that there is a rather common structure of the different models involving a subtle balance between a renormalized viscosity and a renormalized forcing. However, we showed that the latter is rather far from being quasi-Gaussian as hypothesized in the analytical closures or renormalized techniques which failed to obtain its mean field behavior (without rather ad hoc hypothesis) as well as its large fluctuations, i.e. its intermittency. Going well beyond curing the deficiencies, this should give the possibility of deriving analytical/renormalized models of intermittency built on this structure.

Acknowledgments

We heartily thank A. Avez, A. Babiano, M. Larcheveque, H. K. Moffatt and A. M. Yaglom for enlightening discussions. Partial supports by INTAS grant 93-1194 and US DoE ARM Contract KK 4016 are acknowledged.

Appendix A: Increments of a fractionally integrated flux

We first consider the properties of (space) increment of the fractionally integrated field ρ_Λ of a flux F_Λ, defined by Eqs. 21-20:

$$\Delta\rho_{\Lambda,\Delta\underline{x}}(\underline{x}) = \rho_\Lambda(\underline{x}+\Delta\underline{x}) - \rho_\Lambda(\underline{x}) \tag{147}$$

Due to the linearity of the convolution, this increment is the convolution of the same flux F_Λ, but with the increment of the corresponding Green's function, i.e. :

$$\Delta G_{\Delta \underline{x}}(\underline{x}) = G(\Delta \underline{x} + \underline{x}) - G(\underline{x}) \tag{148}$$

To first order we obtain a "dipole effect" at large scale:

$$|\underline{x}| >> |\Delta \underline{x}| \Rightarrow \Delta G_{\Delta \underline{x}}(\underline{x}) \simeq \frac{\underline{x}}{|\underline{x}|} \cdot \Delta \underline{x} \frac{dG(\underline{x})}{d|\underline{x}|} \tag{149}$$

the order of integration for the increment is therefore decreased by one compared to the field ρ_Λ itself, while at small scales we obtain rather a 'unipole effect":

$$|\underline{x} + \Delta \underline{x}| << |\Delta \underline{x}| \quad \Rightarrow \quad \Delta G_{\Delta \underline{x}}(\underline{x} + \Delta \underline{x}) \simeq G(\underline{x} + \Delta \underline{x}) \tag{150}$$

$$|\underline{x}| << |\Delta \underline{x}| \quad \Rightarrow \quad \Delta G_{\Delta \underline{x}}(\underline{x}) \simeq -G(\underline{x}) \tag{151}$$

the increment corresponds to the difference of two independent fields (the domains of integration of the two contributions do not overlap), therefore has the same behavior as the field ρ_Λ. There is therefore a sharp contrast between scales larger and smaller than the space lag. Nevertheless, the scales of the order of $|\Delta \underline{x}|$ yield the main contributions of the convolution corresponding to the two approximations, as soon as both diverge with this scale, i.e. structure functions of order q do scale with $|\Delta \underline{x}|$, as soon as $K(q)$ satisfies:

$$q(H-1)K(q)qH \tag{152}$$

The same considerations hold when considering a generalized scale ($||\underline{x}||$ instead of $|\underline{x}|$),although its gradient (which intervenes in the r.h.s. of Eq. 149 is slightly more involved (due to the fact that the generator $\mathcal{G} \neq \mathbf{1}$). For temporal increments and corresponding causal Green's function (Sec. 4), we have the same phenomenology, although one may rather consider directly the time partial differentiation of this Green's function, which yields in correspondence to Eq 149:

$$|t| >> |\Delta t| \Rightarrow \Delta G_{\Delta t}(\underline{x}, t) \simeq \Delta t \ \partial_t G(\underline{x}, t) \tag{153}$$

Eqs. 150-151 remain rather unchanged.

Appendix B: predictability and auto-decorrelation

We show that, for a space-time causal multifractal field F_Λ, the two measures

$$C_\Lambda^{(1)}(F,\eta,\Delta\underline{x},\Delta t) =< F_\Lambda^\eta(\underline{x},t)\ F_\Lambda^\eta(\underline{x}+\Delta\underline{x},t+\Delta t) > \qquad (154)$$

for a single field F_Λ, and

$$C_\Lambda^{(2)}(F,\eta,\Delta\underline{x},\Delta t) =< F_\Lambda^{(1)\ \eta}(\underline{x},t_0+\Delta t)\ F_\Lambda^{(2)\ \eta}(\underline{x}+\Delta\underline{x},t_0+\Delta t) > \qquad (155)$$

for two fields $F_\Lambda^{(1)}$ and $F_\Lambda^{(2)}$ identical up to time t_0 and diverging after t_0 (for universal multifractals, this can be restated at the subgenerator level: for $t < t_0$, $\gamma^{(1)}(\underline{x},t) = \gamma^{(2)}(\underline{x},t)$, and for $t > t_0$, $\gamma^{(1)}(\underline{x},t)$ and $\gamma^{(2)}(\underline{x},t)$ are two independent realizations of the same white noise), are statistically identical, and characterize two similar processes (the loss of predictability is the consequence of the divergence of a field and its "perturbated" copy, or equivalently the temporal auto-decorrelation of a single field).

Indeed, in the case of $C_\Lambda^{(1)}$, the two terms $F_\Lambda(\underline{x},t)$ and $F_\Lambda(\underline{x}+\Delta\underline{x},t+\Delta t)$ result from the same path of the cascade down to the resolution λ such that $\lambda^{-1} = \|(\Delta\underline{x},\Delta t)\|$. This classical argument (for self-similar fields [17,98,129,130], for self-affine fields [51]) is based on the fact that two structures, at a given resolution, of a cascade are correlated through their common ancestors. The cascading process being Markovian, this correlation is determined by looking at their common ancestor at the largest resolution, thus at resolution $\lambda = \|(\Delta\underline{x},\Delta t)\|^{-1}$. The two remaining paths from λ to Λ are independent (see Fig. 5.5).

On the other hand, the two terms $F_\Lambda^{(1)}(\underline{x},t_0+\Delta t)$ and $F_\Lambda^{(2)}(\underline{x}+\Delta\underline{x},t_0+\Delta t)$ of $C_\Lambda^{(2)}$ can similarly be linked. Let $\lambda' = |\Delta t|^{-1/(1-H)}$ and $\lambda'' = |\Delta\underline{x}|^{-1}$. Indeed, $F_\Lambda^{(1)}(\underline{x},t_0+\Delta t)$ and $F_\Lambda^{(1)}(\underline{x},t_0)$ have their common ancestor $F_{\lambda'}^{(1)}(\underline{x},t_0)$ at maximum resolution λ'; the same observation can be made for $F_\Lambda^{(2)}$, and select $F_{\lambda'}^{(2)}(\underline{x}+\Delta\underline{x},t_0)$ as the common ancestor at maximum resolution. Consider the two extreme cases: (1) $\lambda' >> \lambda''$, then the two structures defined above at resolution λ' are indeed identical, and (2) $\lambda' << \lambda''$, then we need to look to the structures at resolution λ''. The two corresponding structures, $F_{\lambda''}^{(1)}(\underline{x},t_0)$ and $F_{\lambda''}^{(2)}(\underline{x},t_0)$, are identical.

We have shown that the two structures involved in $C_\Lambda^{(2)}$ are correlated through their common ancestor at resolution $\lambda = min\{\lambda',\lambda''\}$, or more directly [r] $\lambda = \|(\Delta\underline{x},\Delta t)\|^{-1}$. Thus $C_\Lambda^{(1)}$ and $C_\Lambda^{(2)}$ both obey the same scaling

[r] the function $max|\Delta\underline{x}|,|\Delta t|^{1/(1-H)}$ is a possible choice for the scale function $\|(\Delta\underline{x},\Delta t)\|$.

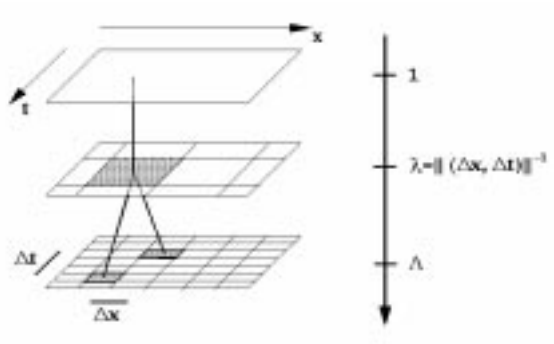

Figure 24: Two structures, at resolution Λ, separated by $(\Delta x, \Delta t)$, are correlated through their common ancestor at maximum resolution $\lambda = ||(\Delta x, \Delta t)||^{-1}$. The two paths, from λ to Λ, are independent.

law [51]:

$$C_\Lambda^{(1)}(F, \eta, \Delta \underline{x}, \Delta t) = C_\Lambda^{(2)}(F, \eta, \Delta \underline{x}, \Delta t) \sim \Lambda^{2K(\eta)} ||(\Delta \underline{x}, \Delta t)||^{-K(2,\eta)} \quad (156)$$

Note that the existence of the cut-off scale is easily deduced from Eq. 156: for $|\Delta \underline{x}| >> |\Delta x_\varepsilon(\Delta t)| \sim |\Delta t|^{\frac{1}{1-H}}$, the correlation measure follows the $|\Delta \underline{x}|^{-K(2,\eta)}$ law, while for $|\Delta \underline{x}| << |\Delta x_\varepsilon(\Delta t)|$ it scales as $|\Delta \underline{x}|^0$: the process can be characterized by the cut-off scale $|\Delta x_\varepsilon(\Delta t)| \sim |\Delta t|^{\frac{1}{1-H}}$.

Appendix C: determination of $\mathcal{E}_\Lambda^{(\eta)}$

We derive the expression of $\mathcal{E}_\Lambda^{(\eta)}$ for the 2-D cut, i.e., $D = 1$, thus 1-D in space and 1-D in time. The extension to higher dimensional case is obvious. $\mathcal{E}_\Lambda^{(2)}$ is the product of a non-causal Green's function $\hat{G}^2(k,\omega)\hat{G}^2(-k,-\omega)$ (see Eq. 90) with a convolution product involving a four-point correlation on the conservative field F_Λ:

$$< \hat{\rho}_\Lambda^2(k,\omega)\hat{\rho}_\Lambda^2(k',\omega') >= \delta(k+k')\delta(\omega+\omega')\ \hat{G}^2(k,\omega)\hat{G}^2(-k,-\omega) \quad (157)$$

$$\times FT[< F_\Lambda^a(0,0)F_\Lambda^a(\Delta x_1, \Delta t_1)F_\Lambda^a(\Delta x_2, \Delta t_2)F_\Lambda^a(\Delta x_3, \Delta t_3) >] \quad (158)$$

where the Fourier Transform (FT) acts on Δx_1, Δx_2, $\Delta x_3 \rightarrow k$ and Δt_1, Δt_2, $\Delta t_3 \rightarrow \omega$. The four-point correlation term can be solved identically as the more traditionnal two-point described above; we find

$$< F^a_\Lambda(0,0)\ F^a_\Lambda(\Delta x_1,\Delta t_1)\ F^a_\Lambda(\Delta x_2,\Delta t_2)\ F^a_\Lambda(\Delta x_3,\Delta t_3) > \tag{159}$$

$$\sim \Lambda^{4K(a)}\ \mathcal{P}[\prod_{n=1}^{3} \|(\Delta x_n,\Delta t_n)\|^{-K(n+1,a)+K(n,a)}] \tag{160}$$

where $\mathcal{P}$ is the operator of permutation on the indexes (6 permutations for 3 indexes). Given the symmetry in the indexes in Eq. 158, we eventually get

$$< \hat{\rho}^2_\Lambda(k,\omega)\hat{\rho}^2_\Lambda(k',\omega') >= \delta(k+k')\delta(\omega+\omega')\ \Lambda^{4K(a)}\ \|(k,\omega)\|^{-4H-3D_{el}-1+K(4,a)} \tag{161}$$

Interpolating this result to all η, we expect $\mathcal{E}^{(\eta)}$ to scale like

$$\mathcal{E}^{(\eta)}_\Lambda(k,\omega) \sim \|(k,\omega)\|^{-2H\eta-2(\eta-1)D_{el}-1+K(2\eta,a)} \tag{162}$$

The terms in the scaling exponent of $\|(k,\omega)\|$ are understood as: (1) $-2H\eta$ is the contribution from the Green's function of Eq. 90; (2) $-2(\eta-1)D_{el}-1$ results from the equivalent of 2η vectorial Fourier Transform (acting on $(\Delta x,\Delta t)$), one leading, due to the invariance by translation, to the δ functions; we then obtain $2\eta-1$ times $-D_{el}$, a scaling in $\|(\Delta x,\Delta t)\|^{-\beta}$ leading to a scaling in the Fourier space in $\|(k,\omega)\|^{-D_{el}+\beta}$; finally, the integration term in $\|(k,\omega)\|^{-D_{el}+1}$ (l.h.s. of Eq. 106) gives the $-2(\eta-1)D_{el}-1$ contribution; and (3) the intermittent correction $K(2\eta,a)$.

References

1. L. F. Richardson, *Weather Prediction by Numerical Processes*, (Cambridge University Press, Cambridge, 1926).
2. L. F. Richardson, *Proc. Roy. Soc.*,**A214**, 1 1926).
3. A. N. Kolmogorov, *Dokl. Acad. Sci. USSR* **30**, 299 (1941).
4. A. M. Obukhov, *Dokl. Akad. Nauk. SSSR* **32**, 22 (1941).
5. M. D. Milliontchikov, *Dokl. Akad. Nauk. SSSR*, **32**, 611 (1941).
6. R. H. Kraichnan, in *Second Symposium on Naval Hydrodynamics* (Office of Naval Research, Washington, 1958).
7. R. H. Kraichnan, *J. Fluid Mech.*, **5**, 82 (1959).
8. D. C. Leslie, *Developments in the theory of turbulence*, (Clarendon Press, Oxford, 1973).
9. M. Lesieur, *Turbulence in Fluids*, (Kluwer, Dordrecht, 1990).
10. D. Forster, D. R. Nelson and M. J. Stephen, *Phys. Rev. A* **16**, 732 (1977).

11. L. Prandtl, *Phys. Zs.* **11**, 1072 (1910).
12. L. D. Landau and E. M. Lifshitz, *Fluids Mechanics*, (Pergamon Press, Oxford, 1987).
13. G. K. Batchelor and A. A. Townsend, *Proc. Roy. Soc.*,**A1 99**, 238 (1949).
14. U. Frisch, M. Lesieur and D. Schertzer, *J. Fluid Mech.* **111**, 127 (1979).
15. A. N. Kolmogorov, *J. Fluid Mech.* **83**, 349 (1962).
16. A. Obukhov, *J. Fluid. Mech.* **13**, 77 (1962).
17. A. M. Yaglom, *Sov. Phys. Dokl.* **2**, 26 (1966).
18. E. N. Lorenz, *J. Atm. Sci.* **20**, 130 (1963).
19. M. Feigenbaum, *Phys. Rev. A* **16**, 732 (1975).
20. P. Grassberger and I. Procaccia, *Phys. Rev. Lett.* **50**, 346 (1983).
21. D. Schertzer and S. Lovejoy, *J. Geoph. Res.*, **92**, 9693 (1987).
22. D. Schertzer, S. Lovejoy and F. Schmitt, in *Small-scale structures in 3D hydro and MHD turbulence*, eds. M. Meneguzzi et al. (Springer-Verlag, Berlin, 1995).
23. D. Schertzer and S. Lovejoy , *J. Appl. Meteor.*, (in press).
24. S. Lovejoy and D. Schertzer, *J. Geophys. Res.*, **95**, 2021 (1990).
25. F. Schmitt, D. Lavallée, D. Schertzer and S. Lovejoy, *Phys. Rev. Letters* **68**, 305 (1992).
26. S. Lovejoy, D. Schertzer, in *Fractals in Geoscience and Remote Sensing*, eds. G. Wilkinson, I. Kanelllopoulous and J. Megier, (Office for Official Publications of the European Communities, Luxembourg, 1995) .
27. Z. She and E. Leveque, *Phys. Rev. Letters* **72**, 336 (1994).
28. E. A. Novikov, *Phys. Rev. E* **50**, R3303 (1994).
29. B. Dubrulle, *Phys. Rev. Letters*,**73**, 959 (1994).
30. Z. She and E. Waymire, *Phys. Rev. Letters* **74**, 262 (1995).
31. H. Fan, *C.R. Acad. Sci. Paris I* **308**, 151 (1989).
32. P. Brax and R. Pechanski, *Phys. Lett. B*, 225 (1991).
33. S. Kida *J. Phys. Soc. of Japan* **60**, 5 (1991).
34. M. Feigenbaum, *Statistical Physics* **46**, 919 (1987).
35. T. Tel, *Z. Naturforsch.* **43**, 1154 (1988).
36. H. G. Schuster, *Deterministic Chaos: an Introduction*, (VCH, New York, 1988).
37. D. Schertzer and S. Lovejoy, in *Fractals, Physical origins and properties*, ed. Pietronero, (Plenum Press, London, 1989).
38. D. Schertzer and S. Lovejoy, *Phys. Rep.*, (in press).
39. E. A. Novikov and R. Stewart, *Izv. Akad. Nauk. SSSR Ser. Geofiz* **3**, 408 (1964).
40. B. Mandelbrot, *J. Fluid Mech.* **62**, 331 (1974).

41. U. Frisch, P. L. Sulem and M. Nelkin, *J. Fluid Mech.* **87**, 719 (1978).
42. D. Schertzer and S. Lovejoy, in *Turbulence and chaotic phenomena in fluids*, ed. T. Tatsumi (North-Holland, 1984).
43. R. Benzi, G. Paladin, G. Parisi and A. Vulpiani, *J. Phys. A* **17**, 3521 (1984).
44. C. Meneveau and K. R. Sreenivasan, *Phys. Rev. Lett.* **59**, 1424 (1987).
45. S. I. Vainshtein, K. R. Sreenivasan, R. T. Pierrehumbert, V. Kashyap and A. Juneja, *Phys. Rev. E* **50**, 1823 (1994).
46. J. Wilson, D. Schertzer and S. Lovejoy *Nonlinear Variability in Geophysics: Scaling and Fractals*, eds. D. Schertzer and S. Lovejoy, (Kluwer, Dordrecht, 1991).
47. D. Schertzer and S. Lovejoy, *Phys. Chem. Hyd. J.* **6**, 623 (1985).
48. S. Pecknold, S. Lovejoy, D. Schertzer, C. Hooge and J. F. Malouin, in *Cellular Automata: Prospects in Astronomy and Astrophysics*, eds. J. M. Perdang and A. Lejeune (World Scientific, Singapore, 1993).
49. S. Pecknold, S. Lovejoy and D. Schertzer, in *Stochastic Models in Geosystems*, eds. S.S Molchan and W.A. Woyczynski, (Springer-Verlag, Berlin, 1996).
50. P. Brenier, D. Schertzer and S. Lovejoy, *Annales Geophysicae*, **Sup.8**, 320 (1991).
51. D. Marsan, D. Schertzer and S. Lovejoy, *J. Geoph. Res.* **101**, 26333 (1996).
52. Y. Chigirinskaya and D. Schertzer, in *Stochastic Models in Geophysics*, eds. A. Molchanov and W. A. Woyczynski (Springer-Verlag, 1996).
53. H. Lamb, *Hydrodynamics,* 6^{th} *Ed.*. (Cambridge University Press, Cambridge, 1963).
54. V. I. Arnold, *Ann. Inst. Fourier (Grenoble)*, **16**, 319 (1966).
55. A. M. Obukhov, *Fluid Dynam. Trans.* **5**, 193 (1971).
56. A. M. Obukhov and E. V. Dolzhansky, *Geoph. Fluid. Dyn.* **6**, 195 (1975).
57. E. B. Gledzer, *Izv. Acad. Nauk USSR Ser. MFG*, **1**, 1980.
58. E. B. Gledzer, E. V. Dolzhansky and A. M. Obukhov, *Systems of fluid mechanical type and their application*, (Nauka, Moscow, 1981), (in Russian).
59. J. R. Herring, D. Schertzer, J. P. Chollet, M. Larchevêque, M. Lesieur and G. R. Newman, *J. Fluid Mech.* **124**, 411 (1982).
60. U. Frisch, *The Legacy of A. N. Kolmogorov*, (Cambridge University Press, 1995).
61. Y. Oono, *Theor. Phys. Suppl.* **99**, 165 (1989).
62. B. Mandelbrot, in *Turbulence and Stochastic Processes*, ed. J. C. R.

Hunt et al., (The Royal Society, London, 1991).
63. G. Parisi and U. Frisch, in *Turbulence and predictability in geophysical fluid dynamics and climate dynamics*, eds. M. Ghil, R. Benzi and G. Parisi (North-Holland, 1985).
64. T. C. Halsey, M. H. Jensen, L. P. Kadanoff, I. Procaccia and B. Shraiman, *Phys. Rev. A* **33**, 1141 (1986).
65. B. Mandelbrot, in *Fractals in the Natural Sciences*, eds. M. Fleischman et al., (Princeton University Press, Princeton, 1989).
66. D. Schertzer and S. Lovejoy, *Physica A* **185**, 187 (1992).
67. V. G. Gupta and E. C. Waymire, *J. Appl. Meteor.*, **32**, 251 (1993).
68. D. Schertzer, S. Lovejoy, D. Lavallée and F. Schmitt, in *Nonlinear Dynamics of Structures*, eds. R. Z. Sagdeev, U. Frisch, A. S. Moiseev and A. Erokhin, (World Scientific, Singapore, 1991).
69. E. Levich and E. Tzvetkov, *Phys. Rep.* **128**, 1 (1985).
70. A. Bialas and R. Peschanski, *Nucl. Phys. B*, **273**, 703 (1986).
71. R. Grauer, J. Krug and C. Marliani, *Phys. Letters A* **195**, 335 (1994).
72. H. Politano and A. Pouquet, *Phys. Rev. E*, submitted, (1994).
73. E. A. Novikov, *Appl. Math. Mech.* **35**, 231 (1971).
74. U. Frisch, in *Turbulence and Stochastic Processes*, ed. by J.C.R. Hunt et al., (The Royal Society, London, 1991).
75. D. Schertzer, S. Lovejoy and D. Lavallée, in *Cellular Automata: Prospects in Astronomy and Astrophysics*, eds. J. M Perdang and A. Lejeune, (World Scientific, Singapore, 1993).
76. S. Lovejoy, D. Schertzer, P. Silas, Y. Tessier and D. Lavallée, *Anna. Geophys.* **11**, 119 (1993).
77. D. Schertzer and S. Lovejoy, *Fractals in the Natural and Applied Sciences*, ed. M. M. Novak, (North Holland, 1994).
78. P. Bak, C. Tang and K. Weiessenfeld, *Phys. Rev. Lett.*, 59, 381 (1987).
79. P. Bak, C. Tang and K. Weiessenfeld, *Phys. Rev. A*, **59**, 364 (1988).
80. D. Lavallée, *Ph. D. thesis*, McGill University, Montreal, Canada (1991).
81. D. Lavallée, S. Lovejoy, D. Schertzer and F. Schmitt, in *Topological Aspects of the Dynamics of Fluids and Plasmas*, eds. K. Moffat, M. Tabor, G. Zalslavsky, M. Tabov and P. Comte (Kluwer, Dordrecht, 1992)
82. D. Lavallee, S. Lovejoy, D. Schertzer and P. Ladoy, *Fractals in Geography*, eds. De Cola and L. Lam (Prentice Hall, 1993).
83. Y. Chigirinskaya, D. Schertzer, S. Lovejoy, A. Lazarev and A. Ordanovich, *Nonlinear Processes in Geophysics*, 1, 105 (1994).
84. A. Juneja, D. Lathrop, K. Seenivasan and G. Solovitzky, *PRE* **49**, 5179 (1994).
85. R. Benzi, L. Biferale, A. Crisanti, G. Paladin, M. Vergassola and A.

Vulpiani, *Physica D* **65**, 352 (1993).
86. A. Marshak, A. Davis, R. Cahalan and W. Wiscombe, *PRE* **49**, 55 (1994).
87. A. Grossmann and J. Morlet, *S.I.AM., J. Math. Anal.* **15**, 723 (1984).
88. I. Daubechies, A. Grossmann and Y. Meyer, *J. Math. Phys.* **27**, 1271 (1986).
89. A. Lazarev, D. Schertzer, S. Lovejoy, and Y. Chigirinskaya, *Nonlinear Processes in Geophysics* **1**, 115 (1994).
90. R. Benzi, S. Ciliberto, R. Tripiccione, C. Baudet, F. Massaioli and S. Succi, *Phys. Rev. E* **48**, R29 (1993).
91. R. Benzi, S. Ciliberto, C. Baudet, G. R. Chavarria and R. Tripiccione, *Europhys. Lett.* **24**, 275 (1993).
92. R. Benzi, S. Ciliberto, C. Baudet and G. R. Chavarria, *Physica D* **80**, 385 (1995).
93. A. N. Kolmogorov, *Dokl. Akad. Nuk. SSSR* **32**, 16 (1941); reprinted in *Proc. R. Soc. Lond.*, **A434**, 15 (1991).
94. R. Benzi, L. Biferale, S. Cliberto, M. Sruglia and R. Tripiccione, *Physica D* **96** 162 (1996).
95. V. Carbone, R. Bruno and P. Veltri, *Nonl. Proc. Geoph.*, in press.
96. A. Obukhov, *Izv. Akad. Nauk SSSR Geogr. I Jeofiz.* **13**, 55 (1949).
97. S. Corrsin, *J. Appl. Phys.* **22**, 469 (1951).
98. A. S. Monin and A. M. Yaglom, *Statistical Fluid Mechanics: Mechanics of Turbulence*, Vol.II (MIT Press, Cambridge, 1975).
99. A. Arneodo et al., *Europhys. Lett.* **34**, 411 (1996).
100. G. Ruiz-Chavarria, C. Baudet and S. Ciliberto, *Europhys. Lett.* **32**, 413 (1995).
101. G. Ruiz-Chavarria, C. Baudet and S. Ciliberto, *Physica D* (in press).
102. R. A. Antonia, E. J. Hopfinger, Y. Gagne and F. Anselmet, *Phys. Rev.* A **30**, 2704 (1984).
103. F. Schmitt, D. Schertzer, S. Lovejoy and Y. Brunet, *Nonlin. Proc. Geophys.* **1**, 95 (1994).
104. J. O. Hinze, *Turbulence*, (McGraw-Hill, New York, 1959).
105. F. Schmitt, D. Schertzer, S. Lovejoy, and Y. Brunet, *Europhys. Lett.* **34**, 195 (1996).
106. F. Schmitt, D. Schertzer, S. Lovejoy, and Y. Brunet, in *Proceedings of the CFIC Conference* ed. M. Giona (World Scientific, Singapore, in press).
107. R. Benzi, L. Biferale and G. Parisi, *Europhys. Lett.* **18**, 213 (1992).
108. F. Schmitt, D. Schertzer and S. Lovejoy, *Geoph. Res. Letters* **22**, 1689 (1995).
109. D. Schertzer and S. Lovejoy, in *Space-Time Variability and Interdependence for Various Hydrological Processes* ed. R. Feddes (Cambridge Uni-

versity Press, Cambridge, 1995).
110. D. K. Lilly in *Turbulence and Predictability in Geophysical Fluid Dynamics and Climate Dynamics*, eds. M. Ghil, R. Benzi and G. Parisi (North-Holland, 1985).
111. P. L. Houtekamer, *Ph. D. thesis*, University of Wageningen, Holland (1992).
112. E. N. Lorenz, *Tellus* **21**, 289 (1969).
113. C. E. Leith and R. H. Kraichnan, *J. Atm. Sci.* **29** 1041 (1972).
114. O. Métais and M. Lesieur, *J. Atm. Sci.* **43**, 9 (1986).
115. A. Crisanti, M. H. Jensen and A. Vulpiani, *Phys. Rev. Letters* **70**, 166 (1993).
116. A. Crisanti, M. H. Jensen, G. Paladin and A. Vulpiani, *J. Phys. A* **26**, 6943 (1993).
117. F. Schmitt, D. Schertzer, S. Lovejoy and Y. Brunet, *Fractals* **1**, 568 (1993).
118. Y. Chigirinskaya, D. Schertzer and S. Lovejoy, in in *Proceedings of the CFIC Conference*, ed. M. Giona (Springer, in press)
119. S. Grossmann and D. Lohse, *Europhys. Lett.* **21**, 201 (1993).
120. V. D. Zimin in *Nonlinear Dynamics of Structures*, eds. R. Z. Sagdeev et al. (World Scientific, Singapore, 1991).
121. B. W. Atkinson, *Mesoscale Atmospheric Circulations*, (Academic Press, London, 1981).
122. I. Orlanski, *Bull. Amer. Met. Soc.* **56**, 527 (1975).
123. G. Taylor, *Proc. R. Soc. Lond. A* **164**, 476 (1938).
124. S. Lovejoy and D. Schertzer, in *Scaling, Fractals and Non-Linear Variability in Geophysics*, eds. D. Schertzer and S. Lovejoy (Kluwer, 1991).
125. V. Gupta and E. Waymire, *J. Geophys. Res.* **92**, 9657 (1987).
126. T. M. Over and V. K. Gupta, *J. Geophys. Res.* **101**, 26319 (1996).
127. R. Lima and R. Vilela Mendes, *Phys. Rev. E* **53**, 3536 (1996).
128. M. Bunge, *Am. Sci.* **49**, 432 (1961).
129. M. E. Cates and J. M. Deutsch, *Phys. Rev. A* **35**, 4907 (1987).
130. J. O'Neil and C. Meneveau, *Phys. Fluid A* **5**, 158 (1993).
131. D. Marsan, D. Schertzer and S. Lovejoy, *Proceedings of the CFIC Conference*, ed. M. Giona (World Scientific, ed. M. Giona, in press).
132. I. Zawadski, *J. Appl. Meteor.* **12**, 459 (1973).
133. R. K. Crane, *J. Geophys. R.* **95**, 2011 (1990).
134. D. Schertzer and S. Lovejoy, *J. Appl. Meteor.* (in press).
135. A. V. Chechkin, D. Schertzer, A. V. Tur and V. V. Yanovsky, *Ukr. J. Phys.* **40**, 434 (1995).